Article

Cell Reports

TDP-43 Regulates Coupled Dendritic mRNA Transport-Translation Processes in Co-operation with FMRP and Staufen1

Graphical Abstract

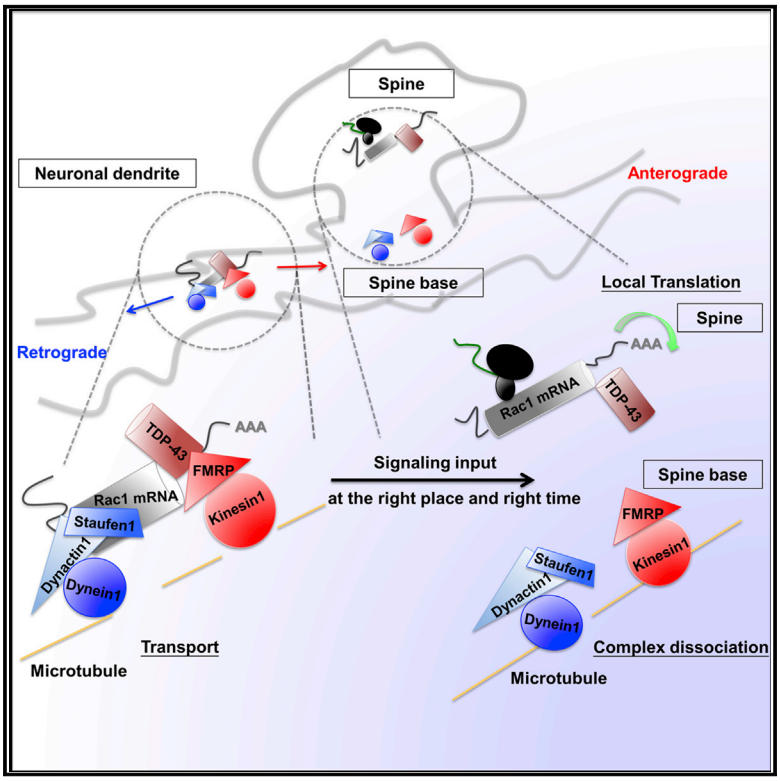

Highlights

- TDP-43 co-operates with FMRP to modulate anterograde transport of dendritic mRNP
- TDP-43 and Staufen1 co-regulate retrograde transport of mRNP in neuronal dendrites
- TDP-43 regulates kinetics and dynamics of coupled dendritic transport-translation
- TDP-43 regulates spine base-to-spine transport of Rac1 mRNA for local translation

Authors

Jen-Fei Chu, Pritha Majumder, Biswanath Chatterjee, Shih-Ling Huang, Che-Kun James Shen

Correspondence

psinp2003@gate.sinica.edu.tw (P.M.), ckshen@imb.sinica.edu.tw (C.-K.J.S.)

In Brief

Chu et al. explore mechanisms of TDP-43-mediated dendritic mRNA transport, combining molecular approaches, real-time imaging, and an RNA biosensor. Analysis of the kinetics and dynamics of coupled transport-translation processes of Rac1 mRNA in neuronal dendrites demonstrates that TDP-43 regulates these processes in cooperation with FMRP and Staufen1 in different subcompartments.

Chu et al., 2019, Cell Reports *29*, 3118–3133
December 3, 2019
https://doi.org/10.1016/j.celrep.2019.10.061

CellPress

OPEN ACCESS
CellPress

Cell Reports
Article

TDP-43 Regulates Coupled Dendritic mRNA Transport-Translation Processes in Co-operation with FMRP and Staufen1

Jen-Fei Chu,[1,2] Pritha Majumder,[1,2,*] Biswanath Chatterjee,[1,2] Shih-Ling Huang,[1] and Che-Kun James Shen[1,3,*]
[1]Institute of Molecular Biology, Academia Sinica, Taipei 115, Taiwan
[2]These authors contributed equally
[3]Lead Contact
*Correspondence: psinp2003@gate.sinica.edu.tw (P.M.), ckshen@imb.sinica.edu.tw (C.-K.J.S.)
https://doi.org/10.1016/j.celrep.2019.10.061

SUMMARY

Tightly regulated transport of messenger ribonucleoprotein (mRNP) granules to diverse locations of dendrites and axons is essential for appropriately timed protein synthesis within distinct sub-neuronal compartments. Perturbations of this regulation lead to various neurological disorders. Using imaging and molecular approaches, we demonstrate how TDP-43 co-operates with two other RNA-binding proteins, FMRP and Staufen1, to regulate the anterograde and retrograde transport, respectively, of Rac1 mRNPs in mouse neuronal dendrites. We also analyze the mechanisms by which TDP-43 mediates coupled mRNA transport-translation processes in dendritic sub-compartments by following in real-time the co-movement of RNA and endogenous fluorescence-tagged protein in neurons and by simultaneous examination of transport/translation dynamics by using an RNA biosensor. This study establishes the pivotal roles of TDP-43 in transporting mRNP granules in dendrites, inhibiting translation inside those granules, and reactivating it once the granules reach the dendritic spines.

INTRODUCTION

Appropriate localization and subsequent local translation of dendritic mRNAs are essential for synaptic plasticity and neuronal development (Buffington et al., 2014; Triller and Sheng, 2012). Various studies have demonstrated that mRNAs are transported in neuronal dendrites and axons as messenger ribonucleoprotein (mRNP) granules containing the mRNAs, RNA-binding proteins (RBPs), translation factors, and ribosomes (Glock et al., 2017; Pilaz and Silver, 2017). Dendritic and axonal mRNPs are associated with cytoskeletal motor proteins, such as kinesins and cytoplasmic dyneins, for long-distance transport along axonal and dendritic microtubules and, in some instances, with myosin motors for transport along actin filaments (Hirokawa and Tanaka, 2015; Xiao et al., 2016). Kinesins mostly facilitate cargo transport in the anterograde direction (Gagnon and Mowry, 2011; Lim et al., 2017). In contrast, dyneins mainly facilitate retrograde transport, but they may also modulate anterograde transport of specific mRNPs in some cell systems (Ayloo et al., 2017; Herbert et al., 2017). Directional transport of mRNP granules is achieved by complex interactions among the mRNAs, RBPs, adaptors, and motor proteins (Buxbaum et al., 2015a; Rezaul et al., 2016).

Dendritic mRNA transport and specific mRNA localization are partly achieved by the co-operative actions of different RBPs (Hutten et al., 2014; Klein et al., 2016). RBPs bind to *cis*-acting elements of mRNAs and can act as direct or indirect adaptors to recruit motor proteins to target mRNPs. TDP-43 and FMRP are RBPs known to regulate dendritic mRNA transport and translation, and functional impairment of either one has been linked to neurodegenerative and neurodevelopmental disorders (Ferro et al., 2018; Richter et al., 2015). FMRP recruits kinesin1 (KIF5) to facilitate dendritic mRNA transport to appropriate locations (Dictenberg et al., 2008). Overexpression of TDP-43 facilitates axonal transport of *Nefl* mRNA in the anterograde direction (Alami et al., 2014). Staufen1 is an RBP that often co-localizes with TDP-43, and FMRP in neuronal dendrites and has been functionally linked with them (Wang et al., 2008; Yu et al., 2012). Moreover, it may associate with dynein through dynactin to facilitate both retrograde and anterograde transport of specific mRNAs in neuronal processes (Gershoni-Emek et al., 2016; Herbert et al., 2017). It is also involved in dendritic mRNA localization and mRNA anchorage to synapses (Gershoni-Emek et al., 2016; Heraud-Farlow and Kiebler, 2014).

mRNA transport and local translation in neuronal processes are closely interlinked. According to the "sushi belt" model, mRNAs masked with RBPs remain translationally inactive or dormant in dendrites until they become unmasked by neuronal activation signals to serve the urgent need for locally translated proteins at synapses/spines (Akbalik and Schuman, 2014; Lee et al., 2016). Mis-regulation of mRNA transport and translation in neuronal processes is closely associated with neurodevelopmental and neurodegenerative diseases, many of which are underpinned by mutations and/or mis-expression of TDP-43 or FMRP (Jovičić and Gitler, 2014; Maziuk et al., 2017).

Here, we conducted time-lapse analysis of dendritic co-movement of an endogenous RBP with one of its endogenous target mRNAs in primary hippocampal neurons as well as pyramidal neurons differentiated from genetically modified mouse embryonic stem cell (mESC) expressing fluorescence-tagged

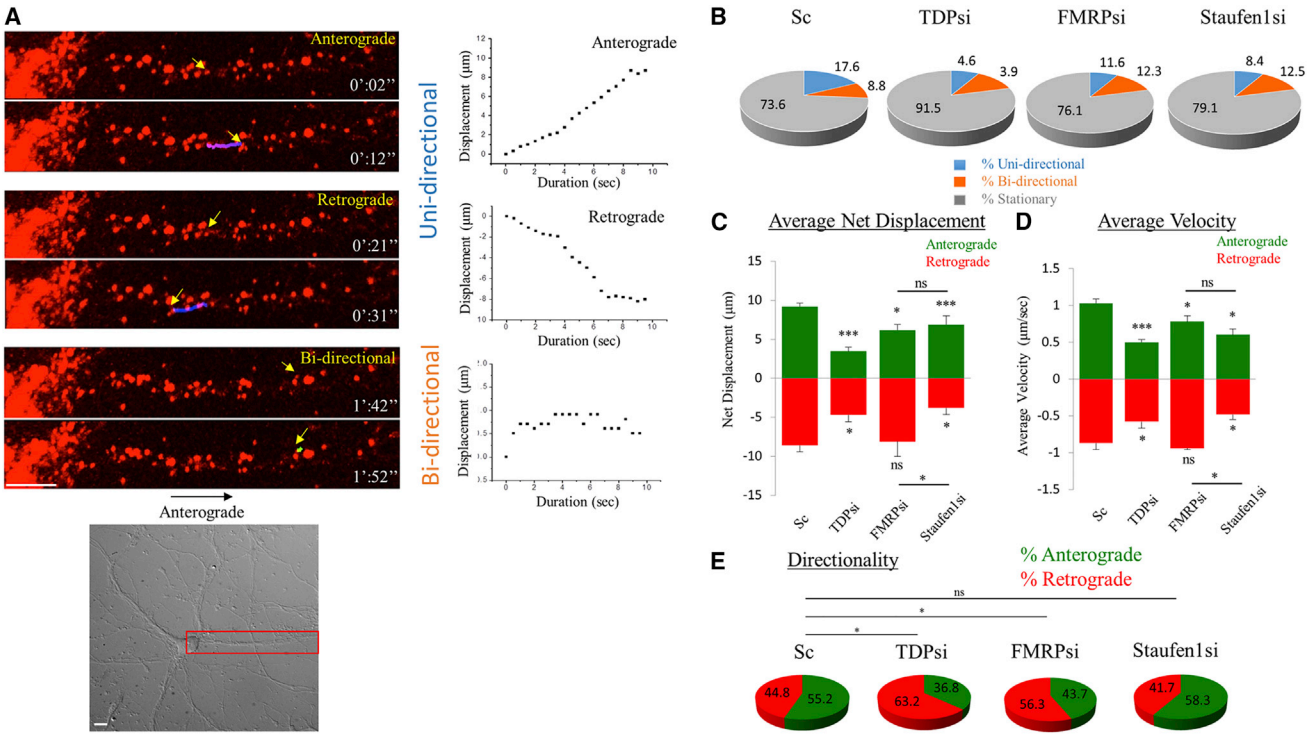

Figure 1. Live-Cell Imaging of Endogenous Rac1 mRNP Granule Transport Dynamics in Primary Hippocampal Neurons

(A) Left, representative real-time images of endogenous Rac1 mRNP granules (arrows with blue and green tracking lines) moving along a selected neuronal dendrite of a DIV14 primary hippocampal neuron (boxed in differential interference contrast [DIC] image at bottom) in the anterograde (away from soma) and retrograde (toward soma) directions or showing bi-directional movement (moving back and forth). Scale bars, 10 μm. Right, representative tracks of three Rac1 mRNP granules exhibiting anterograde, retrograde, or bi-directional displacements along the dendrite within 10 s.

(B) Proportions (%) of stationary, uni-directional, or bi-directional movement by Rac1 mRNP granules (diameter, ≤800 nm) in DIV14 neuronal dendrites transfected with Sc, TDPsi, FMRPsi, or Staufen1si oligos. Note that ~30% of these granules were moving in the Sc condition and decreased significantly upon TDP-43 depletion.

(C and D) Net displacements (C) and average velocities (D) of dendritic Rac1 mRNP granules moving uni-directionally (anterograde, green; retrograde, red) in DIV14 neurons transfected with different RNAi oligos.

(E) Proportions (%) of anterograde or retrograde movement of dendritic Rac1 mRNP granules in neurons transfected with different RNAi oligos. Each set of data derived from 15–30 tracked Rac1 mRNP granules; 6–7 dendrites (technical repeats, n = 6 to 7) examined for each of at least three independent experiments (biological repeats, N ≥ 3). Error bar, SEM. Student's t tests were carried out to compare the means and indicated as *p < 0.05, **p < 0.001, ***p < 0.0001. Fisher's exact test comparing different types of movements of Rac1 mRNP granules from differentially transfected neurons; Sc versus TDPsi, p < 0.0001; Sc versus FMRPsi, p = 0.13041; and Sc versus Staufen1si, p = 0.20339.

TDP-43. Moreover, we provide evidence for the molecular mechanisms by which TDP-43 regulates dendritic mRNA transport in co-operation with FMRP and Staufen1, revealing the functional requirement of TDP-43 as an integral part of the dendritic mRNA transport machinery in the mouse neuronal system. Finally, using an RNA biosensor, we investigated the kinetics and dynamics of simultaneous dendritic mRNA transport and translation, establishing TDP-43 as an essential spatiotemporal regulator of these two processes along dendrites and near spines.

RESULTS

TDP-43, FMRP, and Staufen1 Are Required for Proper Dendritic Trafficking of Endogenous Rac1 mRNA Granules

Endogenous TDP-43, FMRP, and Staufen1 in Mouse Primary Hippocampal Neurons

The association of TDP-43 with FMRP and Staufen1 in dendritic mRNP granules and their increased co-localization upon neuronal activity stimulation (Wang et al., 2008) inspired us to study possible co-regulation of the dendritic transport of motile mRNP granules by these three RBPs. We used time-lapse imaging and molecular beacon probes for live-cell fluorescence *in situ* hybridization (FISH) to study the dynamics of unidirectional/bidirectional/stationary movements of endogenous *Rac1* mRNA within dendrites of 12–14 days *in vitro* (DIV) primary hippocampal neurons (Figures 1A and S1Aa; Video S1), as well as *Rac1* mRNA movement from soma to dendrite or nucleus (Video S1). Proportions of each type of *Rac1* mRNA movement changed significantly upon RNAi-mediated depletion of TDP-43, FMRP, or Staufen1 (Figures 1B and S1B). In particular, under TDP-43 depletion, the percentage of uni-directionally moving granules was reduced (from 17.6% to 4.6%), whereas that of stationary granules increased from 73.6% to 91.5% (Figure 1B). Notably, the average velocity of motile *Rac1* mRNAs was similar to a previous report for *β-actin* mRNA (Park et al., 2014). Although dendritic microtubules remained in place under

TDP-43-depleted conditions (Figure S1C), *Rac1* mRNA motility was reduced dramatically in both the anterograde and retrograde directions compared to the Scrambled RNAi (Sc) control, with marked reductions in net displacement and velocity (Figures 1C, 1D, and S1Ab; Table S1). In contrast, RNAi-mediated depletion of FMRP mainly affected net displacement and velocity of anterograde-moving granules (Figures 1C, 1D, and S1Ac). Depletion of Staufen1, as previously observed for other mRNPs (Vessey et al., 2008), also reduced net displacement and velocity in both directions (Figures 1C, 1D, and S1Ad). Overall, TDP-43 or FMRP depletion led to retrograde-dominant transport of *Rac1* mRNA granules, whereas Staufen1 depletion resulted in anterograde dominance (Figure 1E).

These data demonstrate a pivotal role for TDP-43 in dendritic trafficking of *Rac1* mRNA in primary hippocampal neurons, possibly in co-operation with its binding partners FMRP and Staufen1.

Endogenous RFP-Tagged TDP-43 in Mouse-Embryonic-Stem-Cell-Derived Pyramidal Neurons

To explicitly show that dendritic transport of *Rac1* mRNA required co-localization of endogenous TDP-43 with Rac1 mRNP granules, we used CRISPR/Cas9 genome editing to establish mESC expressing RFP-tagged endogenous TDP-43 protein. These mESC were then transfected with Sc or TDP-43 RNAi (TDPsi) oligos at day 28–32 of differentiation into pyramidal neurons that expressed the specific markers CamKII and PSD-95 (Figures 2A and S2Aa). Expression of RFP-TDP-43 in these mESC-derived neurons was monitored by red RFP fluorescence, most of which was located in the nucleus (Figure S2Ab), whereas endogenous FMRP (Figure S2Ab) was detected by immunostaining using respective antibodies.

Transfected pyramidal neurons were also subjected to time-lapse microscopy at 48 h after transfection to compare the transport dynamics of Rac1 mRNPs (white, *Racl* mRNA beacon) with or without associated endogenous RFP-TDP-43 (red, RFP tag). As exemplified in Figure 2B, most (70%) of the dendritic Rac1 mRNP granules in Sc-oligo-transfected neurons contained the red fluorescently labeled endogenous RFP-TDP-43, which could be effectively depleted (from >90% of all granules) by transfection with a TDPsi oligo. Of these TDP-43-associated Rac1 mRNP granules ((white+red) granules in Figure 2B and Video S2), ~70% were relatively stationary (displacement <1 μm within the 20-s video-recorded tracking period), ~24% of them moved uni-directionally (displacement ≥3 μm within the tracking period), and 5.4% moved bi-directionally with one or more reversals of direction (displacements ≥1 μm in either direction) within the tracking period (left top disc, Figure 2C(a)). Similar results were obtained by tracking RFP-TDP-43 granules (Figure S2B; red granules in Video S3). In contrast, Rac1 mRNP granules not associated with endogenous RFP-TDP-43 in Sc-oligo-transfected neurons (white granules in Figure 2B and Video S2) were either stationary or only moved bi-directionally over short distances.

Slightly more unidirectional TDP-43-associated Rac1 mRNP granules were transported in the anterograde rather than retrograde direction (51.8%, left bottom disc; Figure 2Ca), likely due in part to higher net anterograde displacement (11 versus 4 μm) and higher average anterograde velocity (0.40 versus −0.34 μm/sec) relative to retrograde values (left histobars of Figures 2Cb and 2Cc). However, upon TDP-43 depletion, the percentage of moving Rac1 mRNP granules significantly decreased from ~30% to 15.9%, most of which now moved bi-directionally (top right disc, Figure 2Ca). Furthermore, as observed in primary hippocampal neurons (Figure 1), the movement became retrograde-dominant (bottom right disc, Figure 2Ca), which was associated with considerable reductions in net displacement and velocity in both directions (Table S1; right histobars of Figures 2Cb and 2Cc).

Together, Figures 1 and 2 show that endogenous TDP-43 protein associates with dendritic Rac1 mRNP granules, 70%–80% of which were stationary in neurons and the remaining 20%–30% moved in either the anterograde or retrograde direction. However, TDP-43 depletion caused almost all Rac1 mRNP granules to either remain immobile or to only move bi-directionally over short distances, demonstrating the essential role of TDP-43 in their dendritic transport.

TDP-43 in KCl-Stimulated Mouse Primary Hippocampal Neurons

We also examined the effect of RNAi knockdown of TDP-43 in cultured DIV14 hippocampal neurons with or without KCl stimulation. Repetitive KCl stimulation drives membrane depolarization and mimics neuronal excitation/activation and repetitive learning (Wayman et al., 2006; Wu et al., 2001), which increases the numbers of TDP-43(+) granules and of puncta exhibiting TDP-43+FMRP+Staufen1+RNA co-localization in dendrites of primary neurons (Wang et al., 2008). We found that KCl stimulation increased 2- to 4-fold the amounts of *Rac1* mRNA and *Map1b* mRNA but not *β-actin* mRNA or *Gapdh* mRNA in dendrites (histograms of Figures S3Aa and S3Ab) and by 6- to 7-fold *Rac1* and *Map1b* mRNA levels in dendritic spines/protrusions (histograms of Figures S3Ac and S3Ad). Interestingly, although TDP-43 depletion had no effect on dendritic-to-somatic ratio of mRNA levels in stationary-phase neurons, the KCl-stimulated increases of dendritic/protrusional *Rac1* and *Map1b* mRNAs were greatly abrogated upon transfection with TDPsi oligo (histograms of Figure S3A). Thus, TDP-43 is an essential regulator not only of dendritic transport in steady-state neurons but also of neuronal activity-induced soma-to-dendrite transport of *Rac1* and *Map1b* mRNAs.

Regulatory Mechanisms of mRNP Dendritic Transport by TDP-43 and FMRP

Microtubule-Dependent Dendritic Transport of Rac1 and Map1b mRNAs

Transport of mRNP granules in neurons is known to be microtubule and/or actin filament dependent (Balasanyan and Arnold, 2014; Hancock, 2014). As shown in Figure S3Ba, the increased amounts of dendritic *Rac1* and *Map1b* mRNAs in primary hippocampal neurons upon KCl stimulation could be inhibited by treatment with the microtubule-disrupting reagent nocodazole, but they remained unaffected upon treatment with actin-filament-disrupting cytochalasin D. The transport dynamics of Rac1 mRNP granules was also affected by nocodazole treatment (Figure S3Bb; Table S1). Thus, dendritic

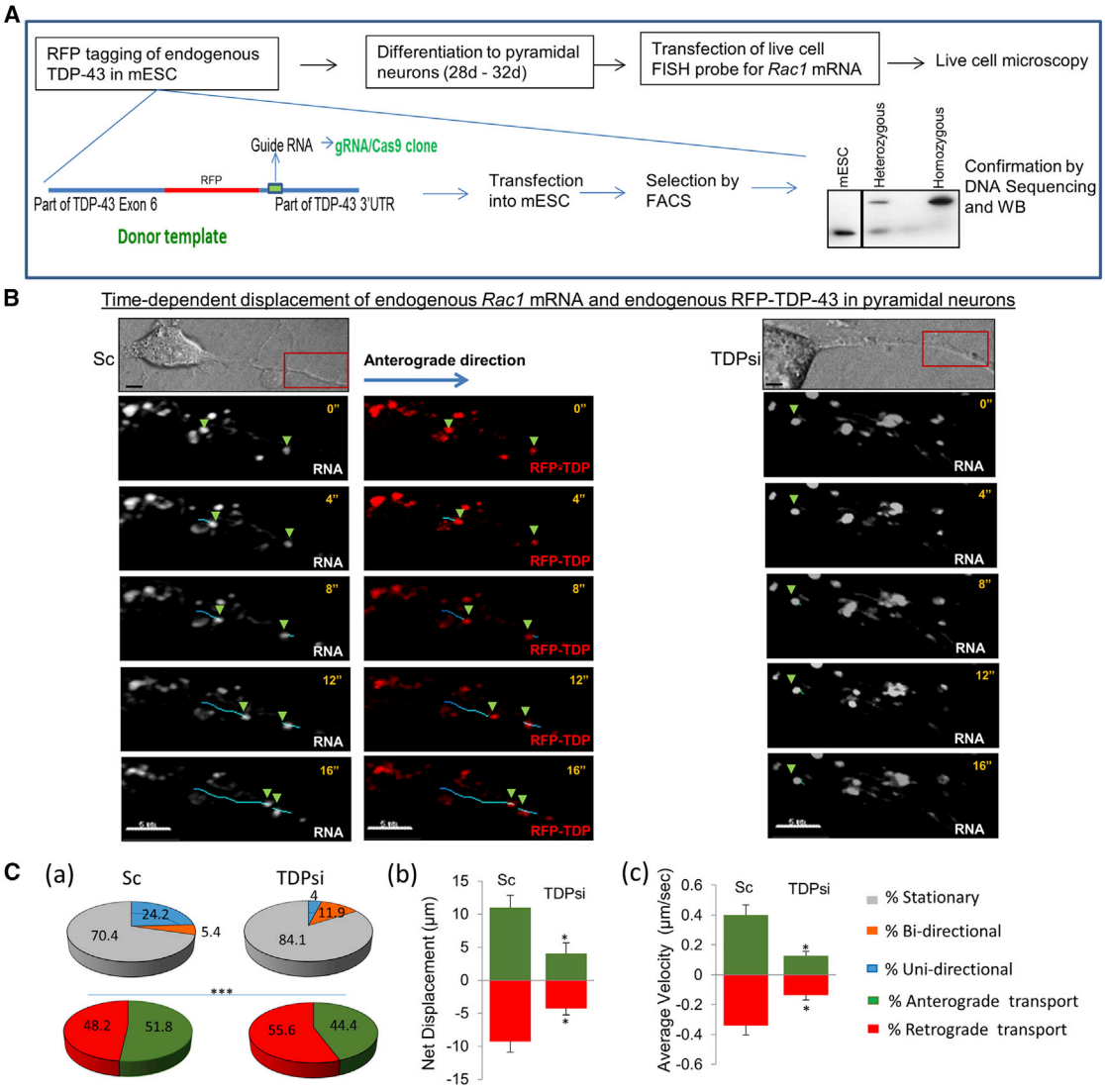

Figure 2. Live-Cell Imaging of Endogenous RFP-TDP-43 and Rac1 mRNP Granule Co-transport in Dendrites of mESC-Derived Pyramidal Neurons

(A) Strategy for generating pyramidal neurons from genetically modified-expressing RFP-tagged TDP-43. A representative western blot image of one homozygous and one heterozygous clone is shown at right.

(B) Representative pictures of time-dependent movements (arrowheads with blue tracking lines) of *Rac1* mRNA (white dots) associated with (Sc condition) and without (TDPsi condition) RFP-TDP-43 (red dots). Corresponding DIC images of the neurons from which specific dendritic regions (red boxes) were chosen for real-time analyses are shown at top. Scale bars, 5 µm. Note that although 67% of RFP-TDP-43 granules were co-localized with *Rac1* mRNA in the exemplified dendrite of Sc-oligo-transfected neurons, on average this co-localization was ~39% (data not shown). Also, >90% of all the granules were without RFP-TDP-43 in TDPsi-transfected cells (RFP channel is not shown in the figure).

(C) Statistical analysis of dendritic transport parameters of (*Rac1* mRNA^{+}TDP-43) granules under the Sc condition and *Rac1* mRNA granules under the TDPsi condition. (a) Proportions (%) of stationary versus bi-directionally moving versus uni-directionally moving granules (top two charts) and of anterograde versus retrograde moving granules (bottom two charts). Comparison of net displacements (b) and average velocities (c) of dendritic *Rac1* mRNAs associated with endogenous RFP-TDP-43 under the Sc condition with those of *Rac1* mRNAs lacking RFP-TDP-43 in TDPsi-transfected neurons. Each set of data represent analysis of 15–40 tracked Rac1 mRNP granules; 3–5 dendrites (technical repeats, n = 3 to 5) were examined for each of three independent experiments (biological repeats, N = 3). Anterograde, retrograde, and bi-directional movements are defined in Figure 1. Error bars, SEM. Student's t tests were carried out to compare the means and indicated as *p < 0.05, **p < 0.001, ***p < 0.0001. Fisher's exact test comparing different types of movements of Rac1 mRNP granules in Sc and TDPsi, represented in pie charts; p < 0.0001. Note, co-movement velocity of Rac1 mRNPs was measured with multiple lasers resulting in a lower time resolution for measurements, so the data cannot be directly compared to single laser-tracking of Rac1 mRNP granules in Figure 1. Tracked endogenous RFP-TDP-43 granules exhibited similar dendritic transport dynamics to Rac1 mRNP granules (compare Figures 1 and S2B).

transport of *Rac1* and *Map1b* mRNAs is predominantly microtubule dependent.

Dendritic Co-localization of Rac1/Map1b mRNAs and RBPs with Kinesin1 and Dynein1

We used combined FISH and immunofluorescence (IF) staining of DIV14 neurons to determine if *Rac1* and *Map1b* mRNAs co-localized with the microtubule-related motor proteins kinesin1 and cytoplasmic dynein1 in the dendrites of stationary-phase neurons. Indeed, we found that kinesin1 co-localized with both *Rac1* mRNA (Figure 3Aa) and *Map1b* mRNA (Figure S3C). Significantly, this co-localization was greatly reduced upon depletion of TDP-43 or FMRP but was unaffected by Staufen1 depletion (left histogram, Figure 3Aa). In addition, dendritic co-localization of TDP-43 and kinesin1 was reduced upon FMRP depletion, but the FMRP and kinesin1 association was independent of TDP-43 (right histogram, Figure 3Aa; representative dendritic pictures shown in Figure S3C). Also, co-localization of dynein1 with *Rac1* mRNA (Figure 3Ab) and *Map1b* mRNA (Figure S3C) was dependent on Staufen1 but not on TDP-43 or FMRP.

Physical Associations among Synaptosomal mRNAs, TDP-43, FMRP, and Kinesin1

Given our immunofluorescence co-staining (co-IF) results, we examined if kinesin1 and dynein1 were physically associated with Rac1/Map1b mRNP complexes by performing an RNA-immunoprecipitation (RNA-IP) assay of synaptosome extracts isolated from KCl-stimulated primary hippocampal neurons transfected with Sc, TDPsi, FMRP RNAi (FMRPsi), or Staufen1 RNAi (Staufen1si) oligos. Synaptosome extracts contain RNAs and proteins from the synaptic vesicles, synaptic membranes, pre-/post-synaptic terminals, synaptodendrosomes, and synaptodendrites (Bai and Witzmann, 2007; Rao and Steward, 1993). KCl treatment enriched *Rac1* and *Map1b* mRNAs in spines/protrusions (Figures S3Ac and S3Ad) and in synaptosomal extracts (Figure S3Da), as reported for other dendritic mRNAs and protein factors (Gharami and Das, 2014; Prieto et al., 2017; Tiruchinapalli et al., 2003). Thus, synaptosomes from KCl-treated primary neurons represent a good resource for isolating sufficient dendritic mRNA complexes for RNA-IP analysis.

In comparison to immunoglobulin G (IgG) control samples, *Rac1* mRNA and *Map1b* mRNA were significantly enriched in anti-kinesin1 and anti-dynein1 immunoprecipitated complexes (Figure 3Ba), indicating an association of these mRNAs with the motor proteins. Furthermore, the associations of kinesin1 with the mRNAs (Figure 3Ba) and with TDP-43 protein (middle panels, Figure 3Bb) were both significantly decreased upon FMRP depletion. However, TDP-43 depletion prompted a significant decrease in the association of kinesin1 with the mRNAs (Figure 3Ba) but not with FMRP protein (middle panels, Figure 3Bb). In contrast, RNAi depletion of Staufen1, but not FMRP or TDP-43, reduced the association of dynein1 with *Rac1* and *Map1b* mRNAs (Figure 3Ba).

Based on these findings and available literature on the physical interactions and co-localizations of FMRP/kinesin1 (Dictenberg et al., 2008), Staufen1/dynein (Gershoni-Emek et al., 2016), TDP-43/FMRP (Majumder et al., 2016), TDP-43/*Rac1* mRNA (Majumder et al., 2016), and TDP-43/*Map1b* mRNA (Coyne et al., 2014; Majumder et al., 2016), we interpret a scenario whereby TDP-43, in association with FMRP, recruits its target mRNAs to kinesin1 and consequently to microtubules. In contrast, whereas Staufen1 independently recruits dynein1 to the mRNAs, depletion of TDP-43 by RNAi reduced the expression of dynactin1 and dynein1 in neurons by ~60% and ~20%, respectively, as shown by qRT-PCR analysis (Figure S3Db). Together, these regulatory pathways contribute to how TDP-43, FMRP, and Staufen1 modulate the anterograde and retrograde movements of TDP-43-targeted mRNPs in dendrites.

Physical Interactions among TDP-43, FMRP, and Kinesin1 Are Required for Anterograde Dendritic Trafficking of Rac1 mRNP Granules

To establish if regulation of dendritic Rac1 mRNP granule transport by TDP-43 and FMRP (Figures 1 and 3) requires physical interactions between these two factors and kinesin1, as suggested by the data presented in Figure 3, we overexpressed wild-type RFP-TDP-43 and/or GFP-FMRP in DIV14 primary neurons by plasmid transfections (Figure 4). Note the partial co-localization of some red and white granules in Figure 4A is due to instrumental limitations of two-channel measurements and momentary dissociation/re-association of the granules. However, exogenous expression of RFP-TDP-43 and GFP-FMRP increased the average amounts of these proteins associated with mRNP granules (Figure S4Aa). Time-lapse microscopy of transfected neurons, exemplified in Figure 4Aa and statistically analyzed in Figures 4Ab–4Ad, showed that Rac1 mRNP granules co-localized (partially or fully) with RFP-TDP-43 ((white+red) dots in Figure 4Aa and Video S4) increased by ~6% their movement in the anterograde direction and by ~60% their net anterograde displacement relative to Rac1 mRNP granules lacking exogenous RFP-TDP-43 (white dots, Figure 4Aa). This outcome may partly be attributable to the stoichiometric increase of total TDP-43 protein (i.e., endogenous TDP-43 plus exogenous RFP-TDP-43) in the Rac1 mRNPs with exogenous RFP-TDP-43 compared to those lacking it (Figure S4Aa). Overexpression of GFP-FMRP alone did not significantly affect *Rac1* mRNA transport (Table S2), possibly due to FMRP already being present in excess in dendrites of DIV14 primary neurons. However, co-expression of GFP-FMRP with RFP-TDP-43 ((white+red+green) granules in Figure 4B and Video S5) increased the proportion of granules moving anterogradely compared to overexpression of RFP-TDP-43 alone ((white+red) granules, Figure 4B), further supporting the co-operative roles of TDP-43 and FMRP in regulating Rac1 mRNP transport in neurons.

We then analyzed the dynamics of dendritic movement of endogenous *Rac1* mRNA in DIV14 primary neurons overexpressing (pGFP-FMRP+pRFP-TDP-43), (pGFP-FMRP+pRFP-TDP-43ΔGly), (pGFP-FMRPΔD1+pRFP-TDP-43), or (pGFP-FMRPΔD3+pRFP-TDP-43) by time-lapse microscopy (Figure 5). The ΔGly deletion prevents interaction of RFP-TDP-43-ΔGly with endogenous FMRP or exogenous GFP-FMRP (Majumder et al., 2016). The ΔD1 deletion weakens the interaction of GFP-FMRPΔD1 with exogenous TDP-43 (Figure S5A) and likely with endogenous TDP-43 too, although it does not affect FMRPΔD1/kinesin1 binding (Dictenberg et al., 2008). The ΔD3 deletion prevents interaction of FMRPΔD3 with kinesin1 (Dictenberg et al., 2008) but does not affect binding of

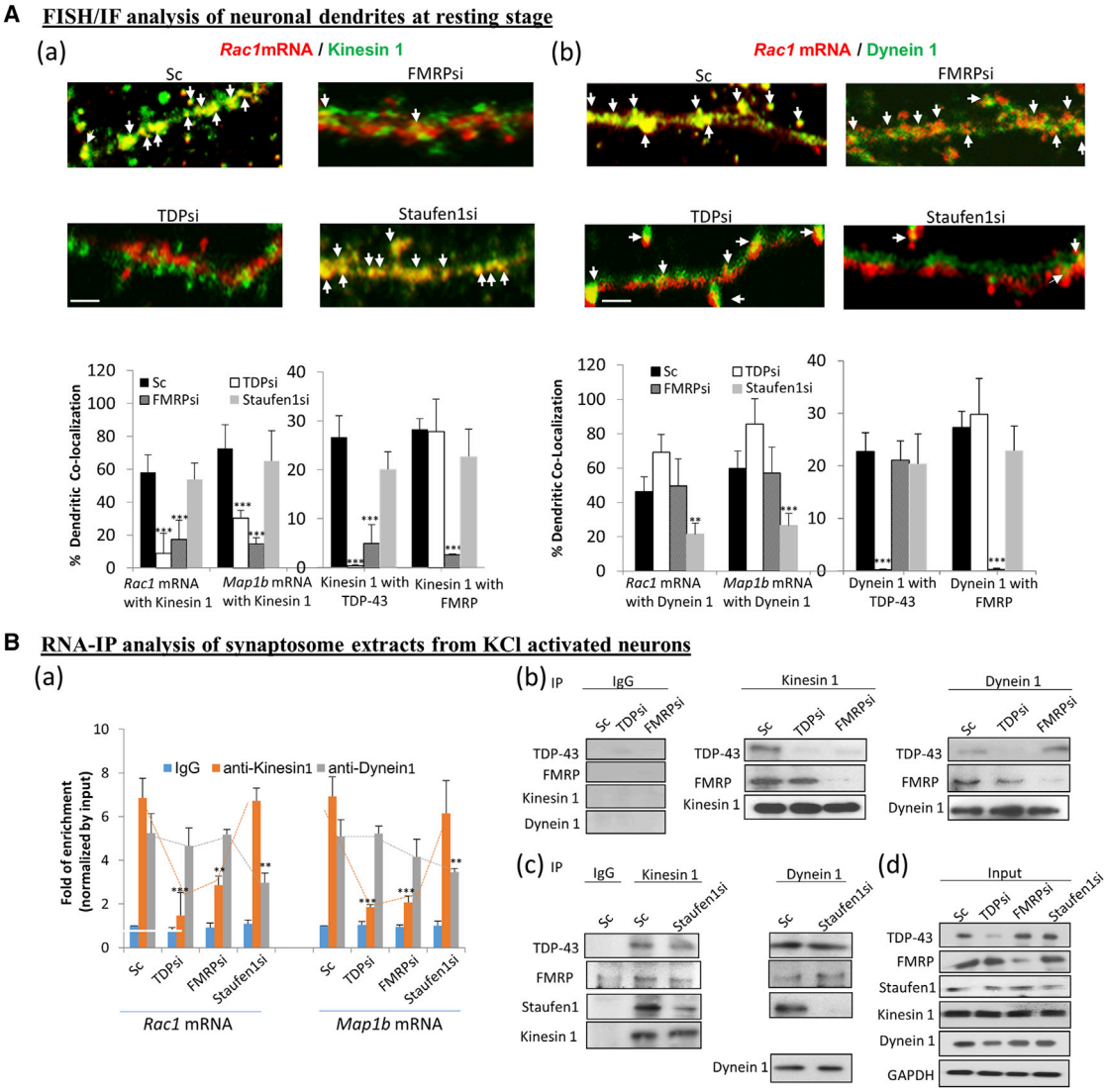

Figure 3. TDP-43-, FMRP-, and Staufen1-Dependent Recruitment of Kinesin1 and Dynein1 to Dendritic Rac1 mRNP Complexes *In Vivo*

(A) Dendritic co-localization of *Rac1* mRNA, *Map1b* mRNA, TDP-43, and FMRP with kinesin1 (a) and dynein1 (b), respectively, in DIV14 primary hippocampal neurons transfected with different RNAi oligos. Hippocampal neurons were subjected to RNA FISH by using probes specific for the mRNAs and co-IF by using anti-TDP-43, anti-FMRP, anti-KIF5A, and anti-dynein1. Representative confocal microscopy images for co-localization of *Rac1* mRNA with kinesin1 and dynein1 are shown in the top panels, with arrows indicating co-localized puncta. Scale bars, 5 μm. Similar representative images for co-localization of *Map1b* mRNA, TDP-43, and FMRP with kinesin1 and dynein1 are shown in Figure S3C. Statistical analysis of co-localization (%) from three sets of independent experiments (biological repeats, N = 3; technical repeats, n = 5 to 6 dendrites for each biological repeat) is represented in the bar diagrams below the image panels.

(B) RNA-IP analysis of synaptosome extracts isolated from DIV14 primary hippocampal neurons after repetitive KCl stimulation. (a) Synaptosome extracts of cultured hippocampal neurons transfected with Sc, TDPsi, FMRPsi, or Staufen1si were immunoprecipitated with different antibodies, and the immunoprecipitated RNAs were analyzed by qRT-PCR (technical repeats, n = 3 for each biological sample) by using primers specific for *Rac1* mRNA and *Map1b* mRNA. The data were normalized with the respective inputs and are presented as fold-enrichment relative to the Sc-IgG control (mean ± SD; N = 5 biological repeats for Sc and TDPsi or N = 3 for FMRPsi or Staufen1si). The immunoprecipitates were also analyzed by western blotting to examine associations of kinesin1 and dynein1 with TDP-43 and FMRP (b and c) and with Staufen1 (c). (d) Inputs showing the different protein levels in synaptosome extracts of the DIV14 primary hippocampal neurons transfected with different siRNA oligos. These IP-western experiments were repeated at least three times (biological repeats, N ≥ 3), and only one set of representative gel pictures is presented in (b), (c), and (d). Student's t tests were carried out to compare the means and indicated as *p < 0.05, **p < 0.001, ***p < 0.0001.

GFP-FMRPΔD3 with exogenous TDP-43 or likely with endogenous TDP-43 either (Figure S5A). Both FMRPΔD1 and FMRPΔD3 can still associate with RNAs (Fernández et al., 2013). As expected, percentages of *Rac1* mRNA co-localization with exogenous TDP-43 (either wild-type RFP-TDP-43 or RFP-TDP-43ΔGly) were similar among the four sets of transfected neurons (left set of four bars, Figure S5B). In contrast, co-localization of *Rac1* mRNA simultaneously with both RFP- and GFP-tagged proteins was exceedingly low in neurons co-expressing either (GFP-FMRP+RFP-TDP-43-ΔGly) or

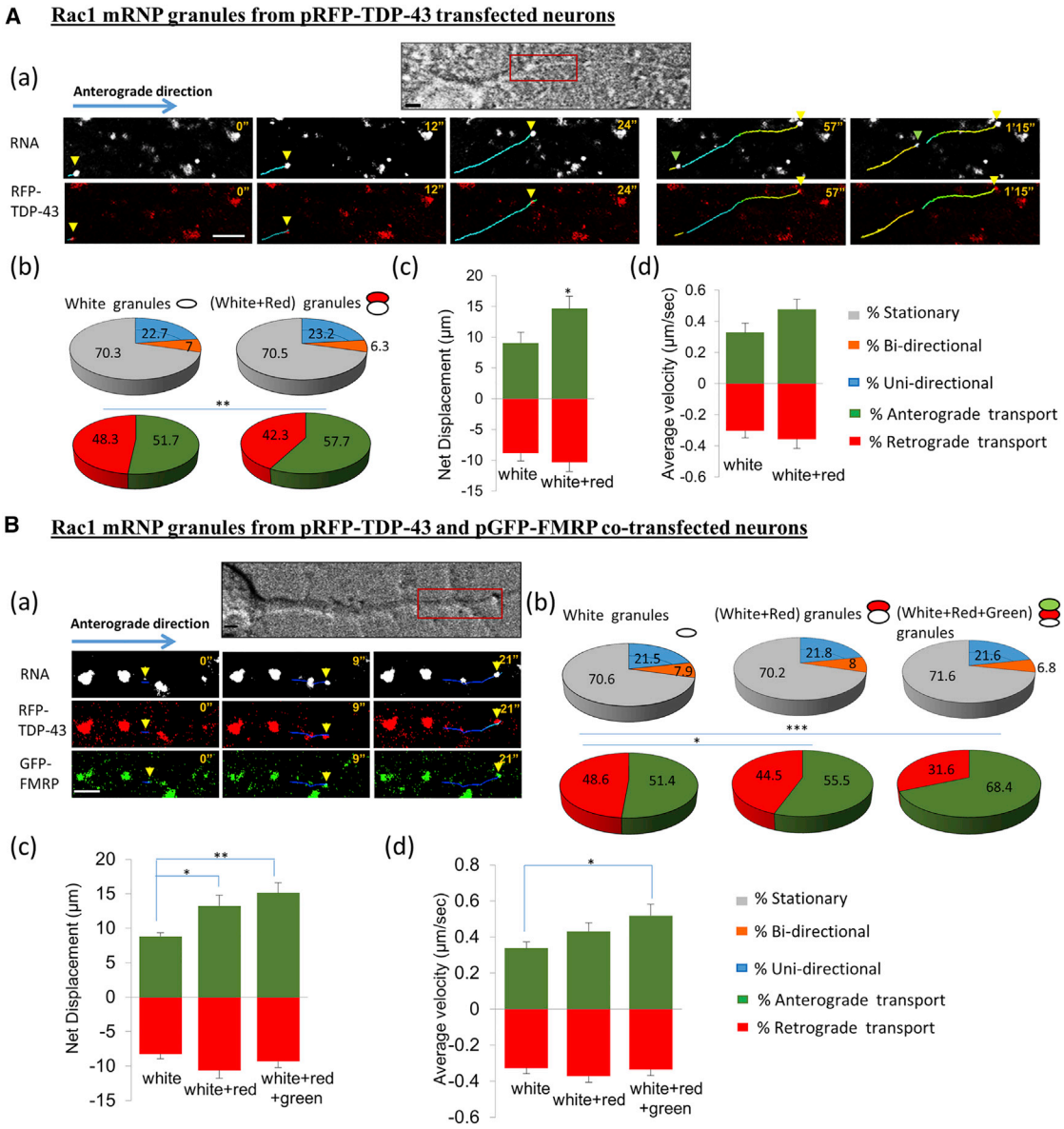

Figure 4. Effects of Exogenous TDP-43 and Exogenous FMRP on the Transport Dynamics of Dendritic mRNP Granules

(A) Live-cell microscopy of the transport dynamics of *Rac1* mRNP granules in pRFP-TDP-43-transfected DIV14 primary hippocampal neurons. (a) Representative images of the time-dependent movements (arrowheads with blue/green/yellow tracking lines) of dendritic *Rac1* mRNP granules (white) with (yellow arrowhead) or without (green arrowhead) associated exogenous RFP-TDP-43 protein (red). Corresponding DIC image is shown at top. Scale bars, 5 µm. (b) Pie charts comparing different movement types. The net displacements and average velocities of uni-directionally moving Rac1 mRNPs are compared in (c) and (d), respectively. Fisher's exact test on data from pie charts; $p = 0.1865$.

(B) Live-cell microscopy of the transport dynamics of Rac1 mRNP granules in pRFP-TDP-43 and pGFP-FMRP co-transfected DIV14 primary hippocampal neurons. (a) Representative images of the time-dependent movement (arrowheads with blue tracking lines) of a dendritic Rac1 mRNP granule (white) associated with both exogenous RFP-TDP-43 protein (red) and GFP-FMRP protein (green). Corresponding DIC image is shown at top. Scale bars, 5 µm. (b) Comparison of different movement types. (c) Comparison of net displacements. (d) Comparison of average velocities. Anterograde, retrograde, and bi-directional movements are defined in Figure 1. Each dataset represents 25–30 tracked Rac1 mRNP granules; 5–6 dendrites (technical repeats, $n = 5$ to 6) were examined for each of five independent experiments (biological repeats, $N = 5$). Different types of Rac1 mRNP granules are represented schematically above pie charts. Fisher's exact test on data from pie charts; white versus (white+red) granules, $p = 0.2927$ and white versus (white+red+green) granules, $p < 0.01$. Error bars, SEM. Student's t tests were carried out to compare the means and indicated as $^*p < 0.05$, $^{**}p < 0.001$, $^{***}p < 0.0001$. Note that although most endogenous (Figures S1B and S2Ab) and exogenous (data not shown) RFP-TDP-43 protein stays in the nucleus, significantly more TDP-43 protein (endogenous TDP-43 + exogenous RFP-TDP-43) was present in both the (white+red) granules and (white+red+green) granules analyzed in (A) and (B), respectively, than in the white or (white+green) granules (Figure S4Aa), helping to recruit more exogenous GFP-FMRP protein to mRNP granules (Figure S4Ab).

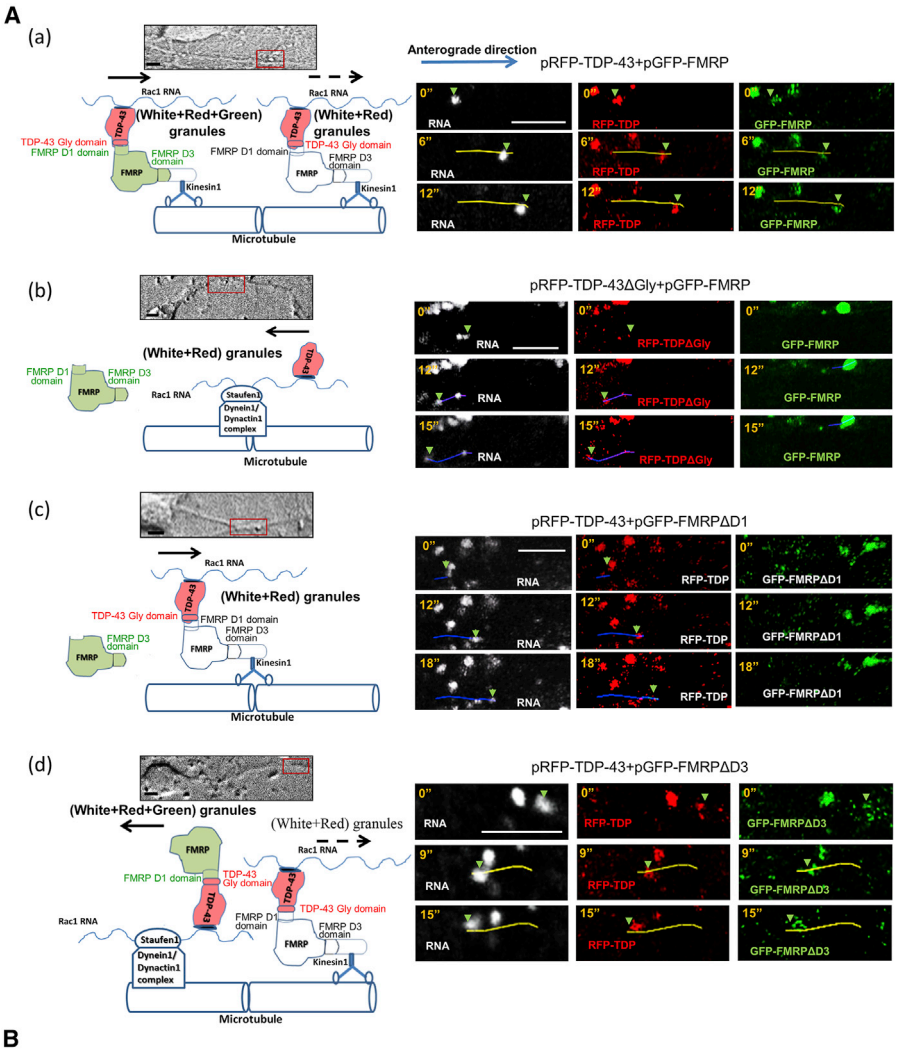

(legend on next page)

(GFP-FMRPΔD1+RFP-TDP-43) (right set of four bars, Figure S5B), making it difficult to examine the transport properties of tri-colored *Rac1* mRNA granules in these two sets of transfected neurons.

Statistical analysis of the transport dynamics of mRNP granules associated with wild-type and mutant forms of exogenous TDP-43 and FMPR proteins is shown in Figure 5B. In contrast to the wild-type system, red-fluorescing Rac1 mRNP granules in neurons co-expressing (GFP-FMRP+RFP-TDP-43ΔGly) or (GFP-FMRPΔD3+RFP-TDP-43) exhibited bi-directional or retrograde-dominant movements (Figures 5Ba and 5Bb), with significant decreases in anterograde net displacements and average velocities (Figures 5Bc and 5Bd), supporting the importance of the physical association of TDP-43/FMRP/kinesin1 for TDP-43 and FMRP co-mediated anterograde transport of dendritic *Rac1* mRNA. Interestingly, unlike the other two deletion mutants, the effect of GFP-FMRPΔD1 on transport dynamics could not be detected because of its severely altered binding with Rac1 mRNA-RFP-TDP-43 (white+red) granules and endogenous FMRP binds with the complex instead of it (Figure S5A; models in Figures 5A and 5B). Notably, other complex protein-protein/RNA interactions might also contribute to this observation.

Full-length and RRM-domain-mutated TDP-43 have similar subcellular distribution patterns, with the majority located in the nucleus (Ayala et al., 2008). RRM domains are required for its binding to *Rac1* mRNA by two UG/GU stretches in the *Rac1 3′UTR* region (Majumder et al., 2016). In the absence of this interaction, *Rac1* mRNA cannot associate/co-localize with FMRP (Majumder et al., 2016). Consistently, *Rac1* mRNA in neurons co-expressing exogenous GFP-FMRP and RFP-TDP-43ΔRRM1 or RFP-TDP-43ΔRRM2 exhibited limited association with either of the fluorescence-tagged proteins (data not shown). Moreover, an MS2 RNA reporter harboring the *Rac1 3′UTR* with disrupted TDP-43-binding UG/GU sequences (Majumder et al., 2016) showed retrograde-dominant movement and reduced anterograde velocity relative to control (Figure S5C). Together, these findings indicate that physical interaction between TDP-43 and *Rac1* mRNA is necessary for anterograde trafficking of *Rac1* mRNA.

Our data thus far (Figures 1, 2, 3, 4, and 5) suggest a mechanistic scenario in which the FMRP-kinesin1 complex interacts with mRNA-bound TDP-43 to facilitate anterograde movement of dendritic granules containing *Rac1* mRNA and likely a subset of other dendritic mRNAs too.

Link between Dendritic Transport and Local Translation of Rac1 mRNP

Use of a TRICK RNA Reporter System to Track Dendritic Transport and Translation in Neurons

To study the inter-dependence of dendritic mRNA transport and translation in neurons, we adopted the *TRICK* reporter RNA system (Halstead et al., 2015) to simultaneously track the trajectories of motile mRNP granules and analyze the distributions of translating (TL; red) and un-translating (UT; yellow or green) granules (Figures 6, 7, S6, and S7) in dendrites. Similar to endogenous *Rac1* mRNA (Figures 1, 2, 3, 4, and 5), the *TRICK-Rac1 3′UTR* RNA exhibited a TDP-43-dependent and anterograde-dominant movement pattern in hippocampal neuronal dendrites (Figure S6B; Table S3). Under the Sc condition, there were more TL granules (red) in proximal dendrites than in distal dendrites, whereas more UT granules (yellow+green) were located in distal dendrites throughout the 7-min period of live-cell imaging (Figures 6A–6C; Video S6; Table S4). Furthermore, we observed a time-dependent decline in UT proportions in proximal dendrites but not in distal ones (Figure 6C; Table S4), perhaps due to the preferential transport of UT granules into distal dendrites (Table S4). Under the TDPsi condition, the population of UT granules decreased in the distal part of dendrites with time, partly due to their decreased anterograde movement upon TDP-43 depletion (Figure S6Bb). Significantly, TDP-43 depletion also caused an 8-fold reduction (from 13.6 min to 1.7 min; Figure 6D) in the average time required for yellow UT reporter RNA granules to become red TL ones. The lack of visible

Figure 5. Live-Cell Imaging Establishes a Requirement for Both the TDP-43/FMRP and FMRP/Kinesin1 Interactions for Anterograde Transport of Dendritic *Rac1* mRNA Granules

(A) Left, schematic representation of dendritic Rac1 mRNP granules containing exogenously expressed wild-type and mutant TDP-43 and/or FMRP proteins in DIV14 primary hippocampal neurons transfected with (a) (pRFP-TDP-43+pGFP-FMRP), (b) (pRFP-TDP-43ΔGly+pGFP-FMRP), (c) (pRFP-TDP-43+pGFP-FMRPΔD1), or (d) (pRFP-TDP-43+pGFP-FMRPΔD3). Exogenous proteins are indicated by red and green colors according to their tagged fluorescent proteins. Endogenous proteins are not colored. As indicated, the D1 domain of FMRP binds TDP-43, and its D3 domain binds kinesin1. Also, the Gly domain of TDP-43 binds FMRP. Solid arrows indicate the direction of movements for *Rac1* mRNA complexes shown in the diagrams and exemplified in the images at right. Broken arrows represent the direction of movements of complexes shown only in the diagram but not shown in representative images at right, as they are not the predominant complexes formed in those cases. DIC images of the dendrites from which specific parts (red boxes) were chosen for live-cell image analysis are shown above individual cartoons. Right, representative images showing time-dependent movements of specific dendritic Rac1 mRNP granules (arrowheads with blue/yellow tracking lines) associated with (a) RFP-TDP-43 and GFP-FMRP (white+red+green), (b) RFP-TDP-43ΔGly (white+red), (c) RFP-TDP-43 (white+red), or (d) RFP-TDP-43 and GFP-FMRPΔD3 (white+red+green) in DIV14 primary hippocampal neurons transfected with different plasmid combinations, as indicated above each set of panels. Scale bars, 5 μm.

(B) Quantitative analysis of transport dynamics. (a and b) Proportions (%) of stationary versus bi-directionally moving versus uni-directionally moving Rac1 mRNP granules (top) and anterograde versus retrograde movement among the uni-directionally moving Rac1 mRNP granules (bottom) among different sets of transfected neurons as described in (A). (c and d) Net displacements and average velocities of different sets of uni-directionally moving Rac1 mRNP granules depicted in (A). The different types of Rac1 mRNP granules analyzed are indicated by colored circles below the pie charts and above individual bars of histograms. Anterograde, retrograde, and bi-directional movements are defined in Figure 1. Each dataset was derived from 18–25 tracked Rac1 mRNP granules; 3–6 dendrites (technical repeats, n = 3 to 6) were examined for each of five independent experiments (biological repeats, N = 5). Error bars, SEM. Student's t tests were carried out to compare the means and indicated as *$p < 0.05$, **$p < 0.001$, ***$p < 0.0001$. Fisher's exact test on data from pie charts; (pRFP-TDP-43+pGFP-FMRP) versus (pRFP-TDP-43ΔGly+pGFP-FMRP), (pRFP-TDP-43+pGFP-FMRPΔD1), and (pRFP-TDP-43+pGFP-FMRPΔD3); $p < 0.001$, $p = 0.2642$, and $p < 0.0001$, respectively.

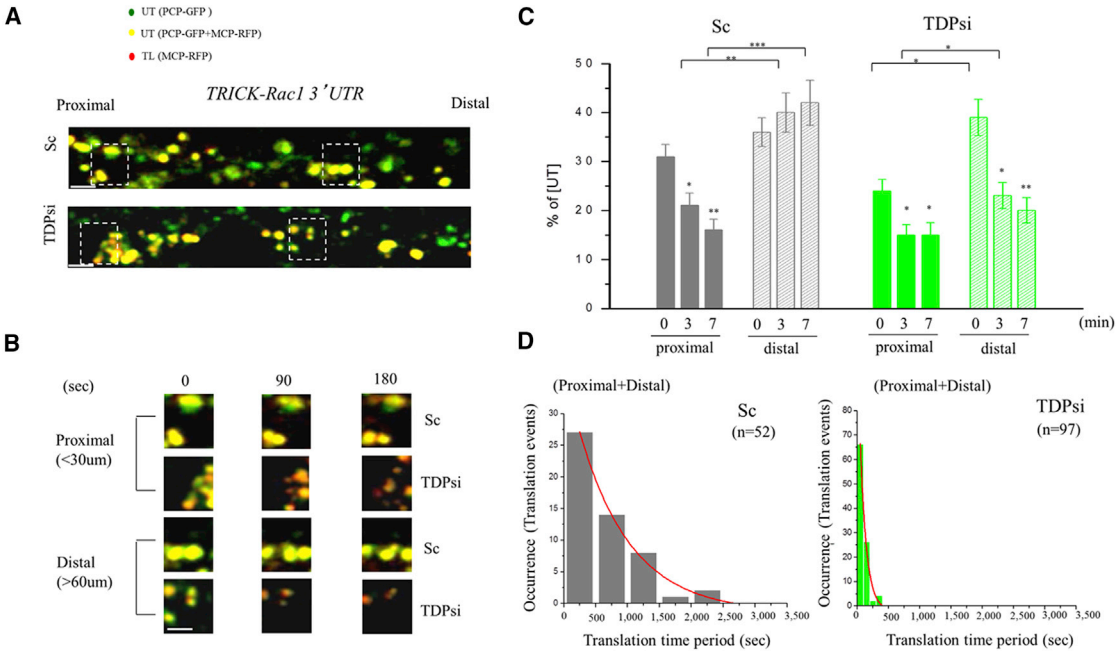

Figure 6. Live-Cell Imaging Analysis of Dendritic Transport and Translation of *TRICK-Rac1 3′UTR* Reporter RNA Granules

(A) Representative images of dendrites of Sc- (top panel) and TDPsi-transfected (bottom panel) DIV14 neurons showing the distributions of un-translating (UT; yellow and green dots) and translating (TL; red dots) *TRICK-Rac1 3′UTR* reporter RNA granules.

(B) Magnified images of the boxed regions in (A) during a recording time period of 180 s. Scale bars, 5 μm. Note most of green dots are UT granules, as they are also associated with the red MCP-RFP protein as verified by visualizing raw images by using two separate channels.

(C) Comparison of altered distributions of UT granules in the proximal and distal parts of dendrites of Sc oligo- (left set) and TDPsi oligo-transfected neurons (right set) during a 7-min recording period. Each dataset was derived from 40–50 reporter RNA granules; 6–7 dendrites (technical repeats, n = 6 to 7) were examined for each of at least three independent experiments (biological repeats, N ≥ 3). Error bars, SEM. Student's t tests were carried out to compare the means and indicated as *p < 0.05, **p < 0.001, ***p < 0.0001.

(D) Translation dynamics of *TRICK-Rac1 3′UTR* reporter RNA granules in Sc oligo- (left panel) and TDPsi oligo-transfected neurons (right panel). Histograms show reduced occurrence of translation events during a 3,500-s recording period. The slope of the curves represents the average translation time for *TRICK-Rac1 3′UTR* reporter RNA granules (from UT [yellow] to TL [red]). Technical repeats (n, number of granules), 52 and 97 for Sc- and TDPsi oligo-transfected neurons, respectively. Data represent at least three independent experiments (biological repeats, N ≥ 3).

TL granules and the robust decrease of UT→TL events within the 7-min tracking period in neuronal dendrites treated with the translation inhibitor cyclohexamide (CHX) confirmed the specificity of our experiments (Figure S6Ca). Furthermore, as deduced from our previous study of the physical interaction between endogenous *Rac1* mRNA and TDP-43 (Majumder et al., 2016), co-localization/physical interaction between the *TRICK-Rac1 3′UTR* reporter RNA and TDP-43 also required the Rac1-3′ UTR sequence (Figures S6Cb, S6Cc, and S6D). These data demonstrate the feasibility of using the *TRICK-Rac1 3′UTR* reporter RNA to analyze TDP-43-mediated mRNP granule transport and translation in neuronal dendrites.

Transport-Coupled Translation in Neuronal Sub-compartments

Translation of dendritic mRNAs primarily occurs inside dendritic spines to facilitate synapse function (Klein et al., 2016; Rangaraju et al., 2017). We used reporter fluorescence to elucidate the role of TDP-43 in the spatial transport and distribution of Rac1 mRNP granules in different sub-compartments of fixed neurons (Figure 7A; Table S5). As observed for the endogenous *Rac1* mRNA (Figure S3Aa), the average number of dendritic reporter RNA granules/μm also remained unaffected after TDP-43 depletion (Figure S7A). However, as shown in Figure 7Ab and Table S5, TDP-43 depletion shifted the distribution of reporter RNA granules from spines (decreased from 51% to 23%) to dendrites (increased from 49% to 77%). Interestingly, accompanying this shifted distribution, the proportion of TL *TRICK* reporter RNA granules in dendrites also increased more than 4-fold, and most of these granules were translated without reaching the spine base (Figure 7Ac; Table S5). These data provide further support for the requirement of TDP-43 to maintain at least some dendritic mRNA granules in the silent state of translation until they reach the spines for "localized translation."

TDP-43-Regulated Reporter RNA Transport and Translation in the Spine Area

The contrasting increase and decrease of reporter RNA granules in dendrites and spines, respectively, upon TDPsi transfection (Figure 7Ab; Table S5) indicated a requirement for TDP-43 to transport dendritic RNA granules into spines. Co-IF analysis of TDP-43, FMRP, and Staufen1 proteins with the *TRICK-Rac1 3′UTR* reporter RNA granules around the spine area (Figure 7B) showed that FMRP- or Staufen1-containing granules were mostly (~70%–80%) distributed at the spine bases. However, reporter RNP granules associated with TDP-43 were somewhat

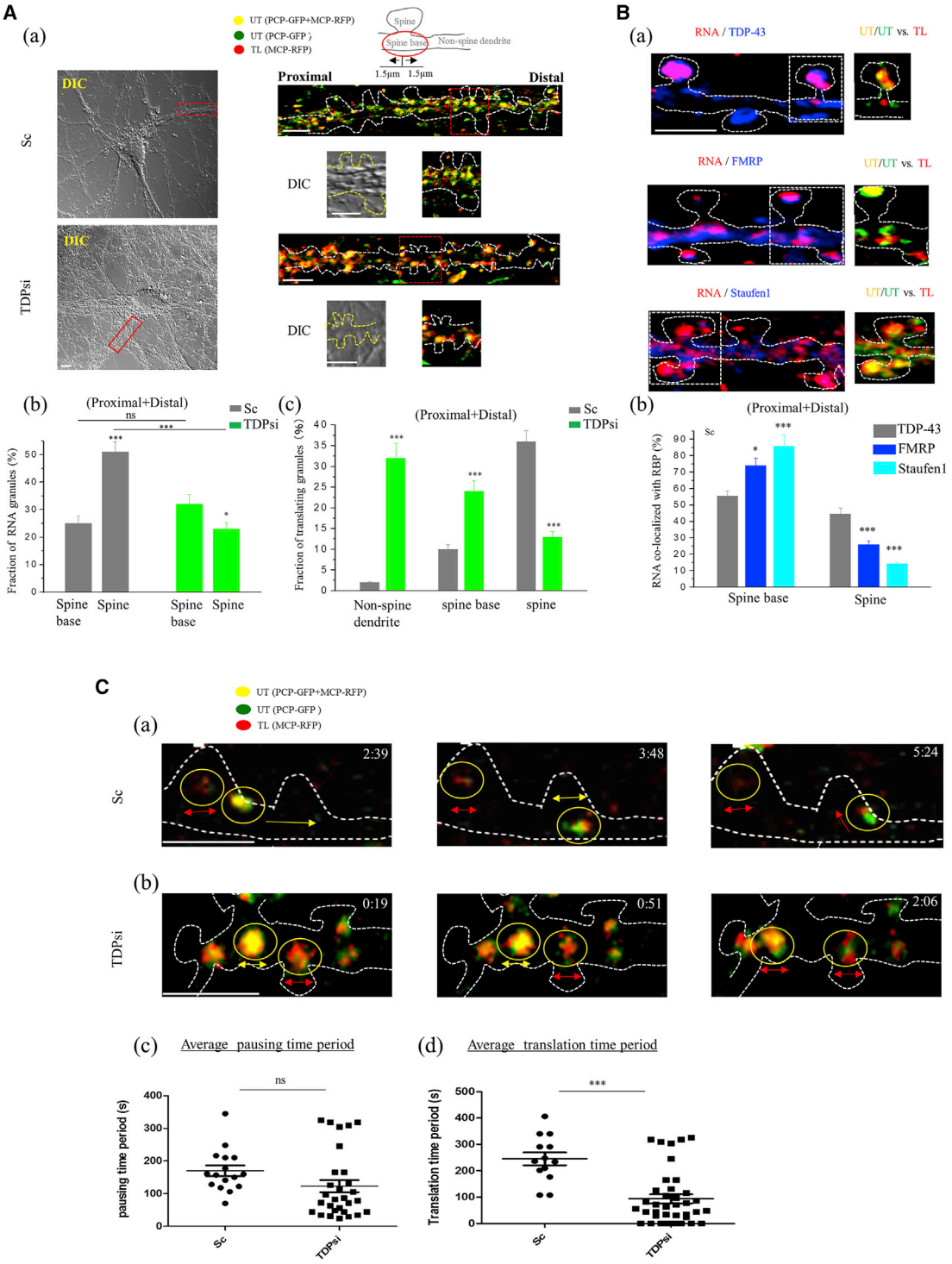

Figure 7. Live-Cell Imaging of Dendritic Transport-Coupled Translation of *TRICK-Rac1 3′UTR* Reporter RNA in Primary Hippocampal Neurons

(A) (a) Representative images showing the distributions of TL and UT reporter mRNP granules in dendrites of DIV14 primary hippocampal neurons transfected with Sc oligo (top panels) or TDPsi oligo (bottom panels). DIC images of the DIV14 neurons are shown at left, with boxed regions indicating dendrites selected for further analysis. Magnified views of dendritic regions show the distributions of UT (green and yellow) and TL (red) granules inside the dendritic morphologies indicated by the white dashed lines. Boxed regions in the magnified fluorescence images are further magnified for better visualization of the translation status of granules in the different dendritic sub-compartments, i.e., non-spine dendrite, spine base, and spine. Scale bars, 5 μm. Note that although the numbers of

(legend continued on next page)

evenly distributed in the spine bases (55%) and inside the spines (45%). Thus, it appears that FMRP and Staufenl might leave the reporter RNA granule complexes before the granules enter the spines, whereas TDP-43 might play a role in translocating the reporter RNA granules from the dendritic spine base into the spines, presumably by an actin-based pathway (Schätzle et al., 2018).

To further examine RNA transport and translation around the spine regions, we used real-time imaging to follow the fate of UT granules (yellow) across a 5-μm region near the spine bases, which spanned, on average, two spines. As shown in Video S7 and Table S6, most of the reporter RNA granules (16/26) paused around the spine base for up to ~3 min. Subsequently, almost all of these granules (15/16) moved from the spine base into the spine before 12 of them (12/15) were locally translated over time, as exemplified in Figure 7Ca and statistically analyzed in Figures 7Cc and 7Cd and Table S6. Upon TDP-43 depletion, although many of the reporter RNA granules (29/42) still paused at the spine bases, very few (4/29) moved into the spines (Figures 7Cb, 7Cc, and 7Cd; Table S6). Although there was no significant difference in the pausing duration of RNA granules at the spine base between Sc and TDPsi conditions (Figure 7Cc), TDP-43 depletion significantly ($p < 0.0001$) reduced the proportion of paused granules that subsequently entered the spines (Table S6) and induced overall 2.5-fold faster translation, as depicted by yellow TRICK reporter granules (UT) becoming red (TL) (Figure 7Cd). Together, the data of Figure 7 and Tables S5 and S6 indicate that TDP-43 plays a pivotal role in regulating localized translation as well as transport in the spine area.

DISCUSSION

Although TDP-43 is known to bind many RNAs and to regulate their processing (Buratti and Baralle, 2012; Ferro et al., 2018; Ling et al., 2013), its regulatory roles in mRNA translation and transport in neurons have only been documented recently. As in other cell types (Wang et al., 2002), most endogenous or exogenously expressed TDP-43 in neurons is located in their nuclei (Arnold et al., 2013; Neumann et al., 2006; Walker et al., 2015; Wang et al., 2008). In neurons, cytoplasmic TDP-43 regulates spinogenesis by co-regulating with FMRP the translation of a subset of neuronal mRNAs (Coyne et al., 2014; Majumder et al., 2017). Furthermore, Alami et al. (2014) previously showed that exogenously expressed TDP-43 in motor neuron axons somewhat pushes the transport of *Nefl* mRNA in the anterograde direction. However, direct evidence that endogenous TDP-43 actively participates in mRNA trafficking in neuronal dendrites had been lacking. Key questions also remained regarding the molecular mechanisms underlying TDP-43-mediated mRNA transport and if TDP-43 spatiotemporally co-regulates the neuronal mRNA transport/translation processes. We are especially interested in establishing whether FMRP co-regulates the transport of mRNAs together with TDP-43, particularly in light of their physical and functional associations and co-regulatory roles in dendritic translation (Ferro et al., 2018; Majumder et al., 2016).

In this study, we show that TDP-43 co-operates with FMRP and Staufen 1 to regulate the spatiotemporal transport of a subset of dendritic mRNAs. First, the requirement for TDP-43 in dendritic transport of *Rac1* mRNA is evidenced in mouse primary hippocampal neurons (Figure 1) and pyramidal neurons derived from genetically modified mESC expressing an endogenous RFP-tagged TDP-43 protein (Figure 2), demonstrating dynamic co-movement of endogenous protein and RNA in neuronal dendrites. In particular, we show that Rac1 mRNP granules lacking any associated TDP-43 protein are mostly stationary (84%) or only move bi-directionally over short distances (12%). Furthermore, in this case, the percentage of granules moving uni-directionally is merely 4% and they move in a retrograde-dominant fashion (Figure 2Ca), with significantly lower net displacement and average velocity in either direction than granules associated with endogenous TDP-43 (Figures 2Cb and 2Cc). TDP-43 also appears to regulate repetitive KCl stimulation-mediated dendritic mRNA localization (Figure S3A). Thus, in addition to mRNA translation, TDP-43 also functions as a regulator of dendritic mRNA trafficking. TDP-43 facilitates anterograde transport of Rac1 and probably other mRNP granules in neuronal processes by co-operating with FMRP to

reporter mRNP granules in different dendrites from different sets of experiments varied, the average numbers of granules per μm of dendrites were similar between Sc- and TDPsi-transfected neurons (Figure S7A). (b and c) Effects of RNAi depletion of TDP-43 on the proportions (%) of dendritic *TRICK-Rac1 3′UTR* reporter RNA granules in spine bases/spines (b) and on the TL fractions (%) of reporter RNA granules in different dendritic compartments (c) of DIV14 primary hippocampal neurons.

(B) (a) Representative images of co-localization of the reporter RNA (red, fluorescence from RNA-bound MCP-RFP) with TDP-43 (left top panel), FMRP (left middle panel), and Staufen1 (left bottom panel), respectively. The translation status (i.e., UT [yellow and green, PCP-GFP+MCP-RFP/PCP-GFP] and TL [red, MCP-RFP]) of mRNP granules in the dashed boxes in the three panels is shown at right. Scale bar, 5 μm. (b) Statistical analysis of the proportion (%) of reporter RNA co-localized with individual RBPs at spine bases (left three bars) and in the spines (right three bars). Each dataset shown in (A) and (B) was derived from analyzing 15–40 granules; 6–7 dendrites (technical repeats, n = 6 to 7) were examined for each of three independent experiments (biological repeats, N = 3).

(C) Transport dynamics of the *TRICK-Rac1 3′UTR* reporter RNA in the spine area of neuronal dendrites. Representative time-lapse images of the reporter RNA granules in Sc oligo- (a) or TDPsi oligo-transfected neurons (b) are shown with the dendritic morphologies indicated by a white dashed line. In (a), a stationary TL granule (red, dot in the left yellow circle) exhibits some diffuse movements within a spine throughout the observation period (2:39–5:24), whereas a UT granule (yellow dot in the right yellow circle) initially moved uni-directionally (yellow arrow in the 2:39 panel), then paused at the base of a nearby dendritic spine (dual-headed yellow arrow in the 3:48 panel), before moving into the spine for localized translation (red arrow in the 5:24 panel). Note that in (b), a stationary UT granule (yellow dot in the left yellow circle) exhibits local diffuse movement in the dendrite (dual-headed yellow arrow) and becomes translated in time, whereas a stationary TL RNP granule presents diffuse motion in the spine base (dual-headed red arrow). Scale bars, 5 μm. (c) Statistical comparison of the duration of pausing among mRNP granules in the spine base before entering the spines. Technical repeats (n, number of granules), 16 and 29 for Sc- and TDPsi oligo-transfected neurons, respectively. (d) Quantitative comparison of time taken for yellow UT granules to become red TL granules in spine areas. Technical repeats (n, number of granules), 13 and 38 for Sc- and TDPsi oligo-transfected neurons, respectively. All data represent at least three independent experiments (biological repeats, $N \geq 3$). Error bars, SEM.

recruit kinesin1 to these mRNP granules (Figures 3Aa, S3C, 3Ba, 4, and 5). It is noteworthy that amyotrophic lateral sclerosis (ALS)-causing mutations in TDP-43 (e.g., A315T, M337V, and G298S) negatively affect TDP-43-mediated anterograde axonal transport of mouse *Nefl* or human *NEFL* mRNP granules in mouse cortical neurons or human induced pluripotent stem cell (iPSC)-derived motor neurons (Alami et al., 2014). Because anterograde transport of mRNP granules is mediated through the interaction between the glycine-rich domain of TDP-43 (Majumder et al., 2016) and the D1 domain of FMRP (Figure S5A), we suggest that some of the ALS-associated mutations in the glycine-rich domain may affect the physical association between TDP-43 and FMRP and, consequently, recruitment of TDP-43-bound mRNAs to kinesin1 and microtubules. This indeed could be the case, as implicated by the weaker binding affinity of FMRP toward the mutant TDP-43 (A315T) than to the wild-type TDP-43 (unpublished data).

TDP-43 indirectly and partly facilitates dendritic transport of mRNP granules in the retrograde direction by maintaining sufficient gene expression of dynein1 and dynactin1 (Figure S3Db). Staufen1 recruits dynein1 to mRNP granules (Figures 3Ab, S3C, and 3Ba) independently of TDP-43 to facilitate their retrograde transport by dynein1/dynactin1 complex. Notably, kinesin1 and dynein1 are plus-end- and minus-end-directed motors, respectively, so they promote the transport of mRNAs in opposite directions because these motor proteins are associated with differentially oriented microtubules (Czaplinski, 2014; Lu and Gelfand, 2017). However, TDP-43 joins a group of other RBPs—including FMRP, Satufen1, and DISC1 (Di Liegro et al., 2014; Falley et al., 2009; Tsuboi et al., 2015)—that function to transport different mRNAs in neuronal processes. All of these RBPs form complexes with mRNAs and other proteins to facilitate mRNA transport while keeping mRNA translation in a silent state during transport (Terenzio et al., 2017). Importantly, further investigation using a TDP-43 null background system may provide more insights into the structural/functional aspects of the role of TDP-43 in dendritic mRNA transport.

We extended our study to examine the importance of TDP-43-mediated mRNA transport in localized translation. TDP-43 was previously reported to regulate dendritic translation of *Rac1* and other mRNAs (Majumder et al., 2016), but the dynamics of TDP-43-mediated translation had remained elusive. To simultaneously detect transport and translation phenomena, we adopted the biosensor TRICK to follow the fate of mRNP granules during these two processes in neuronal dendrites (Figures 6, 7, and S7B; Tables S4, S5, and S6; Videos S6 and S7). Other more advanced biosensors, e.g., the Sun-Tag system, have been used to analyze multiple translation rounds of single mRNA transcript(s) (Wang et al., 2016; Wu et al., 2016), but the TRICK system primarily measures the first round of translation of multiple RNAs within individual RNP granules (Halstead et al., 2015). Our approach allowed us to study the transport/translation of RNP granules in real time inside different compartments of neuronal dendrites, as well as the functional requirement of TDP-43 for these two processes. By simultaneously detecting both processes, we could also analyze association/dissociation of RBPs with mRNAs to establish the translation fate of the mRNAs in different dendritic sub-compartments. As reported for other types of RNP granules (Graber et al., 2013; Wu et al., 2016), most *TRICK Rac1 3′UTR* reporter RNA granules in DIV12–14 primary neurons are translationally silent and they are transported over long distances between the proximal and distal dendrites (Figure 6; Video S6). Notably, TDP-43 depletion accelerated translation dynamics 8-fold (Figure 6D) and significantly enhanced translation kinetics (Table S4), most likely by eliminating the translation silencing exerted by TDP-43/FMRP/CYFIP1 (Majumder et al., 2016) and due to faster ribosome entry into mRNP granules upon RBP dissociating from these granules (Dynes and Steward, 2012; Hüttelmaier et al., 2005; Lovci et al., 2016). An almost similar scenario is apparent near the spine bases where FMRP and Staufen1 dissociate from the mRNPs (Figure 7B), which facilitates polyribosomes located at spine bases to attach onto mRNAs. Ribosomal loading may limit the movement of mRNAs near spine bases (Katz et al., 2016), as evidenced by the *TRICK-Rac1 3′UTR* reporter pausing before moving into the spines for translation (Figure 7C; Video S7). This latter short-distance movement of *TRICK* reporter RNA granules may be achieved through synaptic tagging (Akbalik and Schuman, 2014; Buxbaum et al., 2015b). Our real-time data clearly shows the necessity for translation to occur on relatively stationary RNA granules (Figures 7C and S7B; Videos S6 and S7).

Significantly, TDP-43 depletion increases mis-localized dendritic translation due to stalled movement of the reporter RNA granules in dendrites, preventing them from entering spine areas due to impaired microtubule-dependent transport (Figures 1, 2, 3, 4, 5, and S6B) and, to a lesser extent, stalling them at spine bases probably due to impaired base-to-spine transport (Figure 7C; Table S6). Thus, TDP-43 appears to be necessary to maintain long-distance microtubule-dependent transport, to inhibit translation inside the transporting mRNPs (Majumder et al., 2016) and for short distance base-to-spine transport of a subset of dendritic mRNAs, all of which are essential for appropriate localized translation in spines. Interestingly, these functions of TDP-43 are analogous to those of its physical and functional partner FMRP (Majumder et al., 2016; this study) that has been shown previously to also regulate dendritic transport (Buxbaum et al., 2014; Dictenberg et al., 2008), translation inhibition during transport (Chen and Joseph, 2015), and base-to-spine transport (El Fatimy et al., 2016; Ifrim et al., 2015) of mRNPs. In contrast, most (~75%) of the *TRICK-Rac1 3′UTR* reporter RNA granules associated with the FMRP protein remain at the spine base, whereas those associated with TDP-43 are almost equally distributed between the spine base area and inside the spines (Figure 7B), suggesting that FMRP might have no role or a minor role in spine base-to-spine transport of these mRNP granules. Thus, base-to-spine transport of different sets of dendritic mRNAs may depend on different RBPs. Regulation of this short-distance movement of RNA granules into the spines by TDP-43 may involve crosstalk between actin filament remodeling and transient microtubule polymerization (McVicker et al., 2016; Schätzle et al., 2018). Our data on transport and translation dynamics in spine areas further support the important role of TDP-43 in controlling the transport-coupled translation process in dendritic spines (Figure 7C; Table S6).

Notably, mRNP granules are assembled as membraneless organelles in neurons by liquid-liquid phase separation (LLPS)

(Gomes and Shorter, 2018). TDP-43 is known to associate with mRNPs by LLPS (Gasset-Rosa et al., 2019; Shorter, 2019). However, questions remain as to how LLPS may facilitate timely assembly and disassembly of TDP-43-associated mRNPs in dendrites and in spines to direct transport and translation processes, respectively.

In summary, we have used multiple approaches to dissect the molecular mechanisms of TDP-43-mediated mRNA transport and coupling of transport-translation of mRNP granules in neuronal dendrites, in particular those containing *Rac1* mRNA, in co-operation with two other RBPs, namely, FMRP and Staufen1, as depicted in Figure S8. Our study reveals real-time co-movement of endogenous TDP-43 protein and RNA in neuronal processes and also demonstrates simultaneous transport and translation dynamics by using reporter RNAs. This study also provides direct evidence for the regulation of mRNA transport dynamics by TDP-43 in neuronal dendrites and the molecular mechanisms underlying this role. Finally, we show how the transport of dendritic mRNAs modulates their timely translation in spines. Although different mRNAs likely exhibit different RBP-mediated regulation, some elements of the mechanistic scenario we present could be applicable to dendritic mRNA transport and translation in general. Furthermore, the co-operative functions of TDP-43 and FMRP in regulating dendritic transport and transport-coupled spine translation of synaptic mRNAs suggest the existence of common as yet uncharacterized pathophysiological pathways underlying neurodegenerative diseases and neurodevelopmental disorders.

STAR★METHODS

Detailed methods are provided in the online version of this paper and include the following:

- KEY RESOURCES TABLE
- LEAD CONTACT AND MATERIALS AVAILABILITY
- EXPERIMENTAL MODEL AND SUBJECT DETAILS
  - Primary hippocampal neuron culture
  - Mouse embryonic stem cell culture
  - Cell Lines
- METHOD DETAILS
  - Plasmid construction
  - Primary mouse hippocampal neuronal culture and transfection of RNAi oligos and plasmid DNAs
  - Synaptosome extract preparation and RT-qPCR
  - RNA immunoprecipitation (RNA-IP) assay
  - Combined RNA fluorescence *in situ* hybridization and immunofluorescence staining (RNA FISH/IF)
  - Genome editing by CRISPR/Cas9
  - Live-cell imaging
  - Imaging and movie analysis
- QUANTIFICATION AND STATISTICAL ANALYSIS
- DATA AND CODE AVAILABILITY

SUPPLEMENTAL INFORMATION

Supplemental Information can be found online at https://doi.org/10.1016/j.celrep.2019.10.061.

ACKNOWLEDGMENTS

We thank Yi-Shuian Huang (IBMS, Academia Sinica) for her advice during the course of this study. The expertise of Dr. Yu-Chi Chou, Dr. Ching-Wei Cheng, and other members of RNAi core, Academia Sinica facility are greatly appreciated. Kind help, whenever needed, from Sue-Ping Lee and Shu-Mei Huang in the Microscopy Core at IMB, Dr. Po-Yen Lin in the imaging core facility of ICOB, and all members of FACS facility at IMB are greatly appreciated. We sincerely convey our gratitude to Dr. John O'Brien from English Editing Service, IMB, Academia Sinica for his help in editing of the manuscript. This work was supported by the Frontier of Science Award from the Ministry of Science and Technology, Taiwan (R.O.C.) and a Senior Investigator Award from the Academia Sinica, Taipei, Taiwan (R.O.C.).

AUTHOR CONTRIBUTIONS

J.-F.C., P.M., and C.-K.J.S. designed the experiments. P.M. and J.-F.C. did all the imaging experiments. B.C. did the plasmid cloning and generation of genetically modified cells using CRISPR/Cas9 technology, with the help of S.-L.H. P.M. and B.C. did all the molecular biological experiments. P.M. and J.-F.C. did all data analysis. P.M., J.-F.C., and C.-K.J.S. wrote the manuscript.

DECLARATION OF INTERESTS

The authors declare no competing interests.

Received: October 11, 2018
Revised: July 12, 2019
Accepted: October 14, 2019
Published: December 3, 2019

REFERENCES

Akbalik, G., and Schuman, E.M. (2014). Molecular biology. mRNA, live and unmasked. Science *343*, 375–376.

Alami, N.H., Smith, R.B., Carrasco, M.A., Williams, L.A., Winborn, C.S., Han, S.S.W., Kiskinis, E., Winborn, B., Freibaum, B.D., Kanagaraj, A., et al. (2014). Axonal transport of TDP-43 mRNA granules is impaired by ALS-causing mutations. Neuron *81*, 536–543.

Arnold, E.S., Ling, S.C., Huelga, S.C., Lagier-Tourenne, C., Polymenidou, M., Ditsworth, D., Kordasiewicz, H.B., McAlonis-Downes, M., Platoshyn, O., Parone, P.A., et al. (2013). ALS-linked TDP-43 mutations produce aberrant RNA splicing and adult-onset motor neuron disease without aggregation or loss of nuclear TDP-43. Proc. Natl. Acad. Sci. USA *110*, E736–E745.

Ayala, Y.M., Zago, P., D'Ambrogio, A., Xu, Y.F., Petrucelli, L., Buratti, E., and Baralle, F.E. (2008). Structural determinants of the cellular localization and shuttling of TDP-43. J. Cell Sci. *121*, 3778–3785.

Ayloo, S., Guedes-Dias, P., Ghiretti, A.E., and Holzbaur, E.L.F. (2017). Dynein efficiently navigates the dendritic cytoskeleton to drive the retrograde trafficking of BDNF/TrkB signaling endosomes. Mol. Biol. Cell *28*, 2543–2554.

Baas, P.W., Deitch, J.S., Black, M.M., and Banker, G.A. (1988). Polarity orientation of microtubules in hippocampal neurons: uniformity in the axon and nonuniformity in the dendrite. Proc. Natl. Acad. Sci. USA *85*, 8335–8339.

Bai, F., and Witzmann, F.A. (2007). Synaptosome proteomics. Subcell. Biochem. *43*, 77–98.

Balasanyan, V., and Arnold, D.B. (2014). Actin and myosin-dependent localization of mRNA to dendrites. PLoS One *9*, e92349.

Bibel, M., Richter, J., Schrenk, K., Tucker, K.L., Staiger, V., Korte, M., Goetz, M., and Barde, Y.A. (2004). Differentiation of mouse embryonic stem cells into a defined neuronal lineage. Nat. Neurosci. *7*, 1003–1009.

Bibel, M., Richter, J., Lacroix, E., and Barde, Y.A. (2007). Generation of a defined and uniform population of CNS progenitors and neurons from mouse embryonic stem cells. Nat. Protoc. *2*, 1034–1043.

Buffington, S.A., Huang, W., and Costa-Mattioli, M. (2014). Translational control in synaptic plasticity and cognitive dysfunction. Annu. Rev. Neurosci. *37*, 17–38.

Buratti, E., and Baralle, F.E. (2012). TDP-43: gumming up neurons through protein-protein and protein-RNA interactions. Trends Biochem. Sci. *37*, 237–247.

Buxbaum, A.R., Wu, B., and Singer, R.H. (2014). Single β-actin mRNA detection in neurons reveals a mechanism for regulating its translatability. Science *343*, 419–422.

Buxbaum, A.R., Haimovich, G., and Singer, R.H. (2015a). In the right place at the right time: visualizing and understanding mRNA localization. Nat. Rev. Mol. Cell Biol. *16*, 95–109.

Buxbaum, A.R., Yoon, Y.J., Singer, R.H., and Park, H.Y. (2015b). Single-molecule insights into mRNA dynamics in neurons. Trends Cell Biol. *25*, 468–475.

Chen, E., and Joseph, S. (2015). Fragile X mental retardation protein: A paradigm for translational control by RNA-binding proteins. Biochimie *114*, 147–154.

Coyne, A.N., Siddegowda, B.B., Estes, P.S., Johannesmeyer, J., Kovalik, T., Daniel, S.G., Pearson, A., Bowser, R., and Zarnescu, D.C. (2014). Futsch/MAP1B mRNA is a translational target of TDP-43 and is neuroprotective in a Drosophila model of amyotrophic lateral sclerosis. J. Neurosci. *34*, 15962–15974.

Czaplinski, K. (2014). Understanding mRNA trafficking: are we there yet? Semin. Cell Dev. Biol. *32*, 63–70.

Dehmelt, L., Poplawski, G., Hwang, E., and Halpain, S. (2011). NeuriteQuant: an open source toolkit for high content screens of neuronal morphogenesis. BMC Neurosci. *12*, 100.

Di Liegro, C.M., Schiera, G., and Di Liegro, I. (2014). Regulation of mRNA transport, localization and translation in the nervous system of mammals (Review). Int. J. Mol. Med. *33*, 747–762.

Dictenberg, J.B., Swanger, S.A., Antar, L.N., Singer, R.H., and Bassell, G.J. (2008). A direct role for FMRP in activity-dependent dendritic mRNA transport links filopodial-spine morphogenesis to fragile X syndrome. Dev. Cell *14*, 926–939.

Dynes, J.L., and Steward, O. (2012). Arc mRNA docks precisely at the base of individual dendritic spines indicating the existence of a specialized microdomain for synapse-specific mRNA translation. J. Comp. Neurol. *520*, 3105–3119.

El Fatimy, R., Davidovic, L., Tremblay, S., Jaglin, X., Dury, A., Robert, C., De Koninck, P., and Khandjian, E.W. (2016). Tracking the Fragile X Mental Retardation Protein in a Highly Ordered Neuronal RiboNucleoParticles Population: A Link between Stalled Polyribosomes and RNA Granules. PLoS Genet. *12*, e1006192.

Falley, K., Schütt, J., Iglauer, P., Menke, K., Maas, C., Kneussel, M., Kindler, S., Wouters, F.S., Richter, D., and Kreienkamp, H.J. (2009). Shank1 mRNA: dendritic transport by kinesin and translational control by the 5'untranslated region. Traffic *10*, 844–857.

Fernández, E., Rajan, N., and Bagni, C. (2013). The FMRP regulon: from targets to disease convergence. Front. Neurosci. *7*, 191.

Ferro, D., Yao, S., and Zarnescu, D.C. (2018). Dynamic duo - FMRP and TDP-43: Regulating common targets, causing different diseases. Brain Res. *1693*, 37–42.

Gagnon, J.A., and Mowry, K.L. (2011). Molecular motors: directing traffic during RNA localization. Crit. Rev. Biochem. Mol. Biol. *46*, 229–239.

Gasset-Rosa, F., Lu, S., Yu, H., Chen, C., Melamed, Z., Guo, L., Shorter, J., Da Cruz, S., and Cleveland, D.W. (2019). Cytoplasmic TDP-43 De-mixing Independent of Stress Granules Drives Inhibition of Nuclear Import, Loss of Nuclear TDP-43, and Cell Death. Neuron *102*, 339–357.e337.

Gershoni-Emek, N., Mazza, A., Chein, M., Gradus-Pery, T., Xiang, X., Li, K.W., Sharan, R., and Perlson, E. (2016). Proteomic Analysis of Dynein-Interacting Proteins in Amyotrophic Lateral Sclerosis Synaptosomes Reveals Alterations in the RNA-Binding Protein Staufen1. Mol. Cell. Proteomics *15*, 506–522.

Gharami, K., and Das, S. (2014). BDNF local translation in viable synaptosomes: implication in spine maturation. Neurochem. Int. *69*, 28–34.

Glock, C., Heumüller, M., and Schuman, E.M. (2017). mRNA transport & local translation in neurons. Curr. Opin. Neurobiol. *45*, 169–177.

Gomes, E., and Shorter, J. (2018). The molecular language of membraneless organelles. J. Biol. Chem. *294*, 7115–7127.

Graber, T.E., Hébert-Seropian, S., Khoutorsky, A., David, A., Yewdell, J.W., Lacaille, J.C., and Sossin, W.S. (2013). Reactivation of stalled polyribosomes in synaptic plasticity. Proc. Natl. Acad. Sci. USA *110*, 16205–16210.

Halstead, J.M., Lionnet, T., Wilbertz, J.H., Wippich, F., Ephrussi, A., Singer, R.H., and Chao, J.A. (2015). Translation. An RNA biosensor for imaging the first round of translation from single cells to living animals. Science *347*, 1367–1671.

Hancock, W.O. (2014). Bidirectional cargo transport: moving beyond tug of war. Nat. Rev. Mol. Cell Biol. *15*, 615–628.

Heraud-Farlow, J.E., and Kiebler, M.A. (2014). The multifunctional Staufen proteins: conserved roles from neurogenesis to synaptic plasticity. Trends Neurosci. *37*, 470–479.

Herbert, A.L., Fu, M.M., Drerup, C.M., Gray, R.S., Harty, B.L., Ackerman, S.D., O'Reilly-Pol, T., Johnson, S.L., Nechiporuk, A.V., Barres, B.A., and Monk, K.R. (2017). Dynein/dynactin is necessary for anterograde transport of *Mbp* mRNA in oligodendrocytes and for myelination *in vivo*. Proc. Natl. Acad. Sci. USA *114*, E9153–E9162.

Hirokawa, N., and Tanaka, Y. (2015). Kinesin superfamily proteins (KIFs): Various functions and their relevance for important phenomena in life and diseases. Exp. Cell Res. *334*, 16–25.

Hüttelmaier, S., Zenklusen, D., Lederer, M., Dictenberg, J., Lorenz, M., Meng, X., Bassell, G.J., Condeelis, J., and Singer, R.H. (2005). Spatial regulation of beta-actin translation by Src-dependent phosphorylation of ZBP1. Nature *438*, 512–515.

Hutten, S., Sharangdhar, T., and Kiebler, M. (2014). Unmasking the messenger. RNA Biol. *11*, 992–997.

Ifrim, M.F., Williams, K.R., and Bassell, G.J. (2015). Single-Molecule Imaging of PSD-95 mRNA Translation in Dendrites and Its Dysregulation in a Mouse Model of Fragile X Syndrome. J. Neurosci. *35*, 7116–7130.

Jovičić, A., and Gitler, A.D. (2014). TDP-43 in ALS: stay on target…almost there. Neuron *81*, 463–465.

Kapitein, L.C., and Hoogenraad, C.C. (2011). Which way to go? Cytoskeletal organization and polarized transport in neurons. Mol. Cell. Neurosci. *46*, 9–20.

Katz, Z.B., English, B.P., Lionnet, T., Yoon, Y.J., Monnier, N., Ovryn, B., Bathe, M., and Singer, R.H. (2016). Mapping translation 'hot-spots' in live cells by tracking single molecules of mRNA and ribosomes. eLife *5*, e10415.

Khatri, N., Gilbert, J.P., Huo, Y., Sharaflari, R., Nee, M., Qiao, H., and Man, H.Y. (2018). The Autism Protein Ube3A/E6AP Remodels Neuronal Dendritic Arborization via Caspase-Dependent Microtubule Destabilization. J. Neurosci. *38*, 363–378.

Klein, M.E., Monday, H., and Jordan, B.A. (2016). Proteostasis and RNA Binding Proteins in Synaptic Plasticity and in the Pathogenesis of Neuropsychiatric Disorders. Neural Plast. *2016*, 3857934.

Lee, B.H., Bae, S.W., Shim, J.J., Park, S.Y., and Park, H.Y. (2016). Imaging Single-mRNA Localization and Translation in Live Neurons. Mol. Cells *39*, 841–846.

Lim, A., Rechtsteiner, A., and Saxton, W.M. (2017). Two kinesins drive anterograde neuropeptide transport. Mol. Biol. Cell *28*, 3542–3553.

Ling, S.C., Polymenidou, M., and Cleveland, D.W. (2013). Converging mechanisms in ALS and FTD: disrupted RNA and protein homeostasis. Neuron *79*, 416–438.

Lovci, M.T., Bengtson, M.H., and Massirer, K.B. (2016). Post-Translational Modifications and RNA-Binding Proteins. Adv. Exp. Med. Biol. *907*, 297–317.

Lu, W., and Gelfand, V.I. (2017). Moonlighting Motors: Kinesin, Dynein, and Cell Polarity. Trends Cell Biol. *27*, 505–514.

Majumder, P., Chu, J.F., Chatterjee, B., Swamy, K.B., and Shen, C.J. (2016). Co-regulation of mRNA translation by TDP-43 and Fragile X Syndrome protein FMRP. Acta Neuropathol. *132*, 721–738.

Majumder, P., Chatterjee, B., and Shen, C.-K. (2017). Epitranscriptome and FMRP Regulated mRNA Translation. Epigenomes *1*, 11.

Maziuk, B., Ballance, H.I., and Wolozin, B. (2017). Dysregulation of RNA Binding Protein Aggregation in Neurodegenerative Disorders. Front. Mol. Neurosci. *10*, 89.

McVicker, D.P., Awe, A.M., Richters, K.E., Wilson, R.L., Cowdrey, D.A., Hu, X., Chapman, E.R., and Dent, E.W. (2016). Transport of a kinesin-cargo pair along microtubules into dendritic spines undergoing synaptic plasticity. Nat. Commun. *7*, 12741.

Neumann, M., Sampathu, D.M., Kwong, L.K., Truax, A.C., Micsenyi, M.C., Chou, T.T., Bruce, J., Schuck, T., Grossman, M., Clark, C.M., et al. (2006). Ubiquitinated TDP-43 in frontotemporal lobar degeneration and amyotrophic lateral sclerosis. Science *314*, 130–133.

Park, H.Y., Lim, H., Yoon, Y.J., Follenzi, A., Nwokafor, C., Lopez-Jones, M., Meng, X., and Singer, R.H. (2014). Visualization of dynamics of single endogenous mRNA labeled in live mouse. Science *343*, 422–424.

Pilaz, L.J., and Silver, D.L. (2017). Moving messages in the developing brain-emerging roles for mRNA transport and local translation in neural stem cells. FEBS Lett. *591*, 1526–1539.

Prieto, G.A., Trieu, B.H., Dang, C.T., Bilousova, T., Gylys, K.H., Berchtold, N.C., Lynch, G., and Cotman, C.W. (2017). Pharmacological Rescue of Long-Term Potentiation in Alzheimer Diseased Synapses. J. Neurosci. *37*, 1197–1212.

Rangaraju, V., Tom Dieck, S., and Schuman, E.M. (2017). Local translation in neuronal compartments: how local is local? EMBO Rep. *18*, 693–711.

Rao, A., and Steward, O. (1993). Evaluation of RNAs present in synaptodendrosomes: dendritic, glial, and neuronal cell body contribution. J. Neurochem. *61*, 835–844.

Rezaul, K., Gupta, D., Semenova, I., Ikeda, K., Kraikivski, P., Yu, J., Cowan, A., Zaliapin, I., and Rodionov, V. (2016). Engineered Tug-of-War Between Kinesin and Dynein Controls Direction of Microtubule Based Transport In Vivo. Traffic *17*, 475–486.

Richter, J.D., Bassell, G.J., and Klann, E. (2015). Dysregulation and restoration of translational homeostasis in fragile X syndrome. Nat. Rev. Neurosci. *16*, 595–605.

Schätzle, P., Esteves da Silva, M., Tas, R.P., Katrukha, E.A., Hu, H.Y., Wierenga, C.J., Kapitein, L.C., and Hoogenraad, C.C. (2018). Activity-Dependent Actin Remodeling at the Base of Dendritic Spines Promotes Microtubule Entry. Curr. Biol. *28*, 2081–2093.e6.

Shorter, J. (2019). Phase separation of RNA-binding proteins in physiology and disease: An introduction to the JBC Reviews thematic series. J. Biol. Chem. *294*, 7113–7114.

Smafield, T., Pasupuleti, V., Sharma, K., Huganir, R.L., Ye, B., and Zhou, J. (2015). Automatic Dendritic Length Quantification for High Throughput Screening of Mature Neurons. Neuroinformatics *13*, 443–458.

Terenzio, M., Schiavo, G., and Fainzilber, M. (2017). Compartmentalized Signaling in Neurons: From Cell Biology to Neuroscience. Neuron *96*, 667–679.

Tiruchinapalli, D.M., Oleynikov, Y., Kelic, S., Shenoy, S.M., Hartley, A., Stanton, P.K., Singer, R.H., and Bassell, G.J. (2003). Activity-dependent trafficking and dynamic localization of zipcode binding protein 1 and beta-actin mRNA in dendrites and spines of hippocampal neurons. J. Neurosci. *23*, 3251–3261.

Triller, A., and Sheng, M. (2012). Synaptic structure and function. Curr. Opin. Neurobiol. *22*, 363–365.

Tsuboi, D., Kuroda, K., Tanaka, M., Namba, T., Iizuka, Y., Taya, S., Shinoda, T., Hikita, T., Muraoka, S., Iizuka, M., et al. (2015). Disrupted-in-schizophrenia 1 regulates transport of ITPR1 mRNA for synaptic plasticity. Nat. Neurosci. *18*, 698–707.

Vessey, J.P., Macchi, P., Stein, J.M., Mikl, M., Hawker, K.N., Vogelsang, P., Wieczorek, K., Vendra, G., Riefler, J., Tübing, F., et al. (2008). A loss of function allele for murine Staufen1 leads to impairment of dendritic Staufen1-RNP delivery and dendritic spine morphogenesis. Proc. Natl. Acad. Sci. USA *105*, 16374–16379.

Walker, A.K., Spiller, K.J., Ge, G., Zheng, A., Xu, Y., Zhou, M., Tripathy, K., Kwong, L.K., Trojanowski, J.Q., and Lee, V.M. (2015). Functional recovery in new mouse models of ALS/FTLD after clearance of pathological cytoplasmic TDP-43. Acta Neuropathol. *130*, 643–660.

Wang, I.F., Reddy, N.M., and Shen, C.K. (2002). Higher order arrangement of the eukaryotic nuclear bodies. Proc. Natl. Acad. Sci. USA *99*, 13583–13588.

Wang, I.F., Wu, L.S., Chang, H.Y., and Shen, C.K. (2008). TDP-43, the signature protein of FTLD-U, is a neuronal activity-responsive factor. J. Neurochem. *105*, 797–806.

Wang, C., Han, B., Zhou, R., and Zhuang, X. (2016). Real-Time Imaging of Translation on Single mRNA Transcripts in Live Cells. Cell *165*, 990–1001.

Wayman, G.A., Impey, S., Marks, D., Saneyoshi, T., Grant, W.F., Derkach, V., and Soderling, T.R. (2006). Activity-dependent dendritic arborization mediated by CaM-kinase I activation and enhanced CREB-dependent transcription of Wnt-2. Neuron *50*, 897–909.

Wu, G.Y., Deisseroth, K., and Tsien, R.W. (2001). Spaced stimuli stabilize MAPK pathway activation and its effects on dendritic morphology. Nat. Neurosci. *4*, 151–158.

Wu, B., Eliscovich, C., Yoon, Y.J., and Singer, R.H. (2016). Translation dynamics of single mRNAs in live cells and neurons. Science *352*, 1430–1435.

Xiao, Q., Hu, X., Wei, Z., and Tam, K.Y. (2016). Cytoskeleton Molecular Motors: Structures and Their Functions in Neuron. Int. J. Biol. Sci. *12*, 1083–1092.

Yau, K.W., Schätzle, P., Tortosa, E., Pagès, S., Holtmaat, A., Kapitein, L.C., and Hoogenraad, C.C. (2016). Dendrites In Vitro and In Vivo Contain Microtubules of Opposite Polarity and Axon Formation Correlates with Uniform Plus-End-Out Microtubule Orientation. J. Neurosci. *36*, 1071–1085.

Yu, Z., Fan, D., Gui, B., Shi, L., Xuan, C., Shan, L., Wang, Q., Shang, Y., and Wang, Y. (2012). Neurodegeneration-associated TDP-43 interacts with fragile X mental retardation protein (FMRP)/Staufen (STAU1) and regulates SIRT1 expression in neuronal cells. J. Biol. Chem. *287*, 22560–22572.

STAR★METHODS

KEY RESOURCES TABLE

REAGENT or RESOURCE	SOURCE	IDENTIFIER
Antibodies		
KIF5A (kinesin1)	Millipore	Cat# MAB1614
Dynein1	Millipore	Cat# MAB1618
TDP-43	Proteintech	Cat# 12892-1-AP
FMRP	Millipore	Cat# MAB2160
Staufen1	Santa Cruz	Cat# SC-86883
ChAT	Abcam	Cat# AB15468
Synaptophysin	Sigma	Cat# S5768
GluR1	Santa Cruz	Cat#SC-28799
CamKII	Santa Cruz	Cat#SC-5306
PSD-95	Invitrogen	Cat#MA1-046
Flag	Abcam	Cat#AB49763
GFP	Proteintech	Cat# 66002-I-Ig
AlexaFluor 350-conjugated secondary antibody	Life Technologies	Cat#A21081
AlexaFluor 488-conjugated secondary antibody	Life Technologies	Cat#A11001
AlexaFluor 546-conjugated secondary antibody	Life Technologies	Cat#A11003
AlexaFluor 350-conjugated secondary antibody	Life Technologies	Cat#A21245
Normal rabbit IgG	Proteintech	Cat#30000-0-AP
Normal mouse IgG	Proteintech	Cat#10283-1-AP
Chemicals, Peptides, and Recombinant Proteins		
Lipofectamine 2000	Invitrogen	Cat# 11668-500
Cyclohexamide	Sigma	Cat#66-81-9
Nocodazole	Sigma	Cat#31430-18-9
Cytochalasin D	Enzo Life Sciences	Cat#BML-T109
KCl	Merck	Cat No# 7447-40-7
Experimental Models: Cell Lines		
mESC expressing endogenous RFP-TDP-43	This manuscript	N/A
Oligonucleotides		
Alexa 488-conjugated 5′-TTGACTGGTTCA TTGGTTCA-3′ (anti-sense probe against *Rac1* RNA)	Invitrogen	Cat# K8042A02
Alexa 488-conjugated 5′-AGTTCAAATCCTGT GGTGTG-3′ (anti-sense probe against *Map1b* RNA)	Invitrogen	Cat# M5866A02
Cy5-conjugated 5′-GCUCAUUGACUGGU UCAUUGGUUC A[BtndT]GAGC-BHQ3-3′ with a nuclease resistant 2′-O-methylribonucleotide backbone (Rac1 beacon/live cell FISH probe)	Sigma	Cat# WD06587797-011
Scrambled RNAi (Sc) oligo	Ambion	Majumder et al., 2016
TDP-43 RNAi (TDPsi) oligo	Ambion	Majumder et al., 2016
FMRP RNAi (FMRPsi) oligo	Sigma	Majumder et al., 2016
Staufen1 RNAi (Staufen1si) oligo	Dharmacon	This manuscript
Primers/oligos used in molecular cloning, RT-qPCR and CRISPR/Cas9 genome editing	Mission Biotech, Taiwan	This manuscript Table S7
Recombinant DNA		
pFlag-TDP-43	Majumder et al., 2016	N/A
pFlag-TDP-43(ΔGly)	Majumder et al., 2016	N/A
pRFP-TDP-43	This manuscript	N/A

(*Continued on next page*)

Continued

REAGENT or RESOURCE	SOURCE	IDENTIFIER
pRFP-TDP-43(ΔGly)	This manuscript	N/A
pGFP-FMRP	Majumder et al., 2016	N/A
pGFP-FMRPΔD1	This manuscript	N/A
pGFP-FMRPΔD2	This manuscript	N/A
pGFP-FMRPΔD3	This manuscript	N/A
pmax ponA 6xTRICK 24xMS2SL (pTRICK)	Addgene	Cat# 64542
pTRICK-Rac1 3′UTR	This manuscript	N/A
pPCP-GFP	Addgene	Cat# 64539
pMCP-RFP	Addgene	Cat# 64541
pMS2	This manuscript	N/A
pMS2-Rac1 3′UTR	This manuscript	N/A
pMS2-Rac1 3′UTR(2M3M)	This manuscript	N/A
Software and Algorithms		
Imaris x64	Bitplane	Version 8.4.1
Prism5	GraphPad	Version 5.0.2
Stellaris Probe Designer	Biosearch Technology	Website: http://biosearchtech.com
Oligowalk	Dr. David H. Mathews	Website: http://rna.urmc.rochester.edu
mfold	Dr. Michael Zuker	Website: http://unafold.rna.albany.edu

LEAD CONTACT AND MATERIALS AVAILABILITY

Further information and requests of materials used in this research should be directed to the Lead Contact, Prof. C.-K. James Shen (ckshen@gate.sinica.edu.tw). Plasmid DNA constructs generated in this study (indicated in the Key Resources Table) as well as mESC expressing endogenous RFP-TDP-43 will be made available via material transfer agreement (MTA).

EXPERIMENTAL MODEL AND SUBJECT DETAILS

Primary hippocampal neuron culture

Fourteen day pregnant FVB female mice were used to prepare primary neuronal culture following standard procedure and were maintained in 37 °C incubator containing 5% CO_2 for 3 weeks. All pregnant FVB mice were purchased from the National Laboratory Animal Center of Taiwan and maintained in the Animal Facility of the Institute of Molecular Biology (IMB), Academia Sinica, Taiwan. They were housed in a room maintained on a 12 h/12 h light/dark cycle (light on at 7:00 a.m.) with continuous supply of food and water. Experimental procedures for handling the mice were approved by the Institutional Animal Care and Utilization Committee, Academia Sinica, IACUC number 14-12-769.

Mouse embryonic stem cell culture

mESCs was cultured from cryo-preserved vials, bought from ATCC, on feeder MEF cells using DMEM supplemented with fetal calf serum and LIF. Time to time these cells are differentiated to pyramidal neurons following standard procedure.

Cell Lines

HEK293T cells were obtained from ATCC, cultured in DMEM supplemented with 10% fetal bovine serum (FBS) and penicillin/streptomycin solution in a 37 °C incubator containing 5% CO_2.

METHOD DETAILS

Plasmid construction

pEF promoter-based expression plasmids pFlag-TDP-43 and pFlag-TDP-43(ΔGly) encoding Flag-tagged mouse TDP-43 (Tardbp, "GenBank: NM_145556.4") and its glycine rich-domain deletion mutant, as well as pGFP-FMRP encoding GFP-tagged mouse FMRP ("GenBank: NM_008031.3"), have been described previously (Majumder et al., 2016). Using the primers listed in Table S7, wild-type and mutant forms of TDP-43 were cloned into pDsRed C1 vector within the HindIII/BamHI sites to generate pRFP-TDP-43 and pRFP-TDP-43(ΔGly). Different domain deletion mutants of FMRP—namely FMRPΔD1, FMRPΔD2 and FMRPΔD3—were generated by PCR using the primers listed in Table S7 and cloned into pEGFP N2 vector at the SacI/EcoRI sites. To determine which

FMRP domain is required to physically interact with TDP-43, the plasmids were co-transfected in HEK293T cells using lipofectamine 2000 (Invitrogen) following a standard protocol, and immunoprecipitation experiments were carried out as previously described (Dictenberg et al., 2008; Majumder et al., 2016). The RFP-tagged and GFP-tagged plasmids were used in live-cell FISH to study the effect of TDP-43 and FMRP protein expression on mRNA transport.

pBSK (generous gift from Dr. Yi-Shuang Huang's lab, Academia Sinica, Taiwan) contained a sequence (Luc-24X MS2) corresponding to the luciferase (Luc) open reading frame followed by 24 repeats of the MS2 coat protein-binding site under the control of the bacterial T7 promoter. We cloned the Luc-24xMS2 sequence from this plasmid into the mammalian expression vector pCMV-Tag 3B to generate pMS2. The wild-type and mutated form (2M3M, disrupting two UG/GU stretches at the 3′UTR required for TDP-43 binding) were cloned into XhoI/NotI sites of pMS2 downstream of the Luc-24xMS2 sequence to generate pMS2-Rac1 3′UTR and pMS2-Rac1 3′UTR (2M3M). pMS2-Rac1 3′UTR was co-transfected with pMCP-RFP and used to study reporter RNA transport dynamics. pMS2-Rac1 3′UTR (2M3M) was used as a control.

The 3′UTR of Rac1 RNA ("GenBank: NM_009007.2") was also cloned into pmax ponA 6xTRICK 24xMS2SL (pTRICK) plasmid (Addgene, USA) at the AflII/StuI sites to study both transport and translation dynamics of reporter RNA. The TRICK-Rac1 3′UTR physically associates with TDP-43 protein only through the UG/GU repeats in the Rac1 3′UTR. This association is required for translation inhibition of Rac1 mRNA along the dendrites (Majumder et al., 2016). pTRICK expressing a reporter RNA without the Rac1 3′UTR was used as a negative control.

Primary mouse hippocampal neuronal culture and transfection of RNAi oligos and plasmid DNAs

The 14-day-old pregnant FVB mice were obtained from the National Laboratory Animal Center of Taiwan. Preparation of primary hippocampal neuron cultures followed standard protocols described in Majumder et al. (2016). In some cases, primary neuron cultures were subjected to cyclohexamide (Sigma) (100 μg/ml for 30 minutes), nocodazole (Sigma) (1 μg/ml for 10 minutes), or cytochalasin D (Enzo Life Sciences) (1 μg/ml for 10 minutes) treatment and/or repetitive KCl (Merck, Germany) treatment (90 mM for 3 minutes, followed by 5 minutes recovery, with 3 repetitions of this process). For RNAi knockdown, the cultured hippocampal neurons at days *in vitro* (DIV) 12-14 were transfected with different RNAi oligos—TDP-43 RNAi oligo (TDPsi, Ambion), FMRP RNAi oligo (FMRPsi, Sigma), Staufen1 RNAi oligo (Staufen1si, Dharmacon), or control oligo (Sc, Dharmacon)—using lipofectamine 2000 (Invitrogen) following a standard protocol (Majumder et al., 2016). For live-cell FISH analysis with fluorescence-tagged proteins, 4 μg of pRFP-TDP-43 or pGFP-FMRP was transfected alone, or 2 μg of pRFP-TDP-43 or pRFP-TDP-43ΔGly was co-transfected together with 2 μg of pGFP-FMRP or pGFP-FMRPΔD1 or pGFP-FMRPΔD2 or pGFP-FMRPΔD3, using lipofectamine 2000 (Invitrogen) following the same protocol. Twenty-four hours after plasmid transfection, the cells were incubated with 10 nM live-cell FISH probe against Rac1 RNA for another 1 day before starting live-cell imaging. To carry out TRICK reporter RNA experiments, 0.5 μg of pPCP-GFP (Addgene, USA), 1.5 μg of pMCP-RFP (Addgene, USA) and 1 μg of pTRICK-Rac1 3′UTR were co-transfected using a standard procedure.

Synaptosome extract preparation and RT-qPCR

Synaptosome extracts were prepared from hippocampal neurons at DIV 12-14 using SynPer reagent from ThermoScientific (USA) following the user's manual. In brief, cells were lysed in an appropriate amount of SynPer reagent supplemented with protease inhibiter and RNase inhibiter to ensure the integrity of protein and RNA content in the synaptosomes. Cell lysates were then centrifuged at 1200 × g for 10 minutes at 4°C to precipitate the nuclei (discarded), followed by centrifugation of the supernatant at 15,000 × g for 20 minutes at 4°C. The synaptosome pellet was resuspended in SynPer reagent and subjected to western blot (WB) analysis using anti-PSD-95 and compared with crude cell extract to ensure enrichment of these proteins in the synaptosome extract (Figure S3Da).

We carried out RT-qPCR analysis using synaptosome extracts following the method described in Majumder et al. (2016). Total RNA was isolated from synaptosome extracts using the Trizol method, followed by first-strand cDNA synthesis using Superscript RT (Invitrogen) and subjected to real-time PCR using a Light Cycler machine (Roche Biochemical Sciences) with primers for the mouse KIF5A subunit of kinesin1, dynein1, dynactin1 and Gapdh (Table S7).

RNA immunoprecipitation (RNA-IP) assay

RNA-IP experiments were carried out with synaptosome extracts from primary hippocampal neurons as described (Majumder et al., 2016). In brief, the lysates were incubated with anti-KIF5A (Millipore), anti-dynein1 (Millipore), or control IgG antibodies (Jackson Lab, USA) at 4°C overnight to immunoprecipitate the RNA-protein complexes. Agarose beads (GE Healthcare) were used to pull down these complexes and RNAs were extracted from the complexes using TRIZOL (Invitrogen). We then conducted RT-qPCR using the primers listed in Table S7. Another part of the extracts of the pulled down complexes was separated by 10% SDS-PAGE, transferred to membranes, and analyzed by western blotting using anti-TDP-43 (Genetex), anti-FMRP (Millipore), anti-Staufen1 (Santa Cruz Biotechnology), anti- KIF5A (Millipore) and anti-dynein1 (Millipore) antibodies. Note that different parts of membrane(s) were cut according to the molecular weight marker and probed with different antibodies. RNA-IP with HEK293T cells co-transfected with pTRICK or pTRICK-Rac1 3′UTR plasmids along with different RNAi oligos was conducted in the same way.

Combined RNA fluorescence *in situ* hybridization and immunofluorescence staining (RNA FISH/IF)

The RNA FISH probes were designed using the program available from the website of Biosearch Technology. The reliability of the selected probes was tested in the OLIGOWALK and mFold software. Sequence specificities of the selected 3′UTR regions for probe design were checked by BLAST on the NCBI website. Live-cell FISH of Rac1 mRNA was performed using Cy5-conjugated 5′-GCUCAUUGACUGGUUCAUUGGUUC A[BtndT]GAGC-BHQ3-3′ with a nuclease-resistant 2′-O-methylribonucleotide backbone. The probe was prevented from nuclear localization by conjugation to NeutrAvidin. This RNA probe can specifically bind to endogenous Rac1 RNA (Majumder et al., 2016; Figure S1D). Beacons were synthesized with a biotin-modified-dT nucleotide in the 3′ stem sequence and a Cy5 quencher of BHQ3 was conjugated at the 3′ end. RNA FISH was performed using Alexa 488-conjugated 5′-TTGACTGGTTCATTGGTTCA-3′ (anti-sense probe against Rac1 RNA) and 5′-AGTTCAAATCCTGTGGTGTG-3′ (anti-sense probe against Map1b RNA) purchased from Life Technologies (Japan) following the protocol described in Majumder et al. (2016). Simultaneous imaging of RNA by FISH and proteins by IF staining was carried out using standard Biosearch Technology protocols. The FISH probes and antibodies anti-TDP-43 (GeneTex, 1:450), anti-FMRP (Millipore, 1:200), anti-Staufen1 (Santa Cruz Biotechnology, 1:100), anti-KIF5A (Millipore, 1:200) and/or anti-dynein1 (Millipore, 1:250) were mixed and incubated with the neurons overnight at 37°C. The cells were then further incubated with AlexaFluor 488-, AlexaFluor 546-, AlexaFluor 647-, and/or AlexaFluor 350-conjugated secondary antibodies (1:5000 for each, Invitrogen). FISH-IF images were acquired by LSM780 (Zeiss, Germany) confocal microscopy and analyzed by Zen2010 (Zeiss, Germany) and Metamorph (Molecular Devices) software.

Immunofluorescence staining with anti-Map2 (Millipore, 1:100) was used to study microtubule stability in primary hippocampal neurons. Microtubule destabilization by 1 μg/μl nocodazole treatment for 10 minutes, which would cause dendrite retractions and reduce dendritic lengths (Dehmelt et al., 2011; Khatri et al., 2018) visible by Map2 staining (Smafield et al., 2015), was used as a positive control.

Genome editing by CRISPR/Cas9

Cloning of donor plasmid

DNA sequences for the left homology arm (LHA, part of exon 6 of TDP-43) and the right homology arm (RHA, part of the 3′UTR of TDP-43) were amplified from genomic DNA using the primers listed in Table S7. The coding sequence of RFP was PCR-amplified from pDsRed C1 plasmid. These three fragments of DNA were joined together, keeping the coding sequence of RFP in the middle and in-frame with the LHA, using PCR. Final PCR product (size ~900 base pairs) was gel-purified and cloned into pJet2.1 (ThermoFisher Scientific, USA) using a standard procedure.

Cloning of gRNA

Guide RNA (gRNA) oligos were designed using the online CRISPR Design Tool (https://zlab.bio/guide-design-resources) and the one with the least off-target effect was chosen for the next step. Oligonucleotide pairs (Table S7) were hybridized and cloned into pAll-Cas9.pPuro (RNAi Core Facility, Academia Sinica, Taiwan) at the BsmBI site.

Transfection and clone isolation

mESCs were cultured on inactivated MEF cells (feeder) for about 24 hr in ES cell culture medium (DMEM supplemented with 15% FCS, LIF (1:100), 2 mM L-glutamine, non-essential amino acids, 5 ml/500 mL of β-mercaptoethanol) using a standard procedure. Cells, taken up in a cuvette as a suspension culture, were electroporated with the bicistronic gRNA/Cas9 plasmid (10μg) and the donor plasmid (10 μg) at 500V for 2 ms using the Electroporater ECM830 system (BTX). Cells were plated and cultured first for 3 days under puromycin (Thermo Scientific, final concentration 2 μg/ml) and then by culture for ~7 days in medium without puromycin. The cells were then sorted for RFP fusion protein using BD FACS Aria III (BD Biosciences, Heidelberg, Germany) and cultured in a 6 cm format. After a few days, single colonies were isolated under microscopy, cultured in 12-well plate formats, and inspected under fluorescence microscopy to select clones with the highest expression of RFP-tagged protein. At this stage, mESCs from each highly-expressing clone were preserved for further analysis. Finally, DNA and protein were isolated from each of these clones to check the junctions between the 900 bp donor sequence and the genomic DNA between the LHA and RFP CDS, as well as that between the RFP CDS and RHA, using semiquantitative PCR and to examine homozygosity and heterozygosity using WB analysis.

mESC differentiation into pyramidal neurons in culture

Differentiation of mESCs followed the procedure established by Bibel and co-workers (Bibel et al., 2004, 2007). Briefly, mESCs were cultured with ES cell culture medium on plates coated in 0.1% gelatin (Merck, Germany) and without feeder for 2-3 passages before being re-cultured with CA medium (DMEM supplemented with 10% FCS, 2 mM L-glutamine, non-essential amino acids and 5 ml/500 mL β –mercaptoethanol) in bacteriological plates to allow embryonic body (EB) formation. After 4 days, retinoic acid (RA, final concentration 5 μM) was added. EBs were dissociated into single cells on day 8 using a standard procedure with freshly prepared trypsin/EDTA solution. Cells were then re-suspended in N2 medium [125 mL DMEM, 1.25 mL L-glutamine (2 mM), 125 mL F-12, 1.25 mL insulin (25 mg/ml), 6.25 mL transferrin (50 mg/ ml), 0.25 mL progesterone (20 nM), 0.25 mL putrescine (100 nM), 25 mL sodium selenite (30 nM), 1.25 mL BSA (Sigma, 50 mg/ml), and 2.5 mL penicillin/streptomycin] and finally plated on coverslips pre-coated with ornithine (Sigma) and laminin (Sigma). For long-term culture, N2 medium was supplemented with B27 (GIBCO). Staging of the differentiated neurons was done by immunofluorescence-staining using anti-ChAT (Sigma), anti-Synaptophysin (Sigma),

anti-GluR1 (Santa Cruz Biotechnology) and anti-PSD-95 (Sigma), followed by microscopic analysis of the cells at different days in culture (Bibel et al., 2007). For live-cell imaging studies, neurons at 28-32 days of differentiation were used after being transfected with RNAi oligos, e.g., Sc or TDPsi.

Characterization of the pyramidal neurons was carried out by IF using antibodies against pyramidal neuron-specific markers, i.e., CamKII and PSD-95 (Figure S2Aa). These neurons are likely functional and excitable given the repetitive KCl stimulation-mediated increases of TDP-43/FMRP/GluR1 protein puncta (Figure S2Ab) in their dendrites.

Live-cell imaging

Imaging of primary hippocampal neurons was done at DIV 12-14, and that of mESC-derived pyramidal neurons was done at 28-32 days of differentiation. Dendrites of the neurons were chosen over axons primarily on the basis of the presence of spines and protrusions under the microscope and in the DIC images. In some cases, to validate the identity of the dendrites over axons, the cells were fixed after live cell imaging and co-immunostained with anti-Map2 (staining the dendrites) and anti-Tau (staining the axons). Representative microscopic pictures are shown in Figure S4B. Time-lapse movies were obtained using a Spinning-Disc confocal system (Nikon, Japan) associated with a 647 nm solid-state laser (Cobolt) to excite the Cy5 reporter tagged on the endogenous Rac1 mRNA FISH probes, a 561 nm solid-state laser (Cobolt) to excite the RFP reporter of endogenous RFP-TDP-43 protein or exogenous RFP-tagged TDP-43 protein or MCP-RFP in TRICK experiments, or a 488 nm solid-state laser (Coherent) to excite exogenous GFP-tagged FMRP protein or PCP-GFP in TRICK experiments. This approach allowed us to follow the dynamics of endogenous Rac1 mRNA alone or together with endogenous/exogenous RBPs or to track the translation dynamics of Rac1 reporter RNA using the TRICK system. For all experiments, imaging was conducted using a Nikon 60x or 100x 1.4NA objective lens, with cells being maintained at 37°C and 5% CO2 (FC-5N CO2 controller) throughout the LCI TC chamber (Korea), with the alto-focus system turned on during the recording of time-lapse images. In live-cell FISH experiments to follow endogenous Rac1 mRNA, the recording time-period was 5 min, whereas in our translation kinetics study and in the experiments in which we followed translation dynamics using the TRICK system, the recording time-periods were 7 min and 30-60 min, respectively. For all the experiments with one laser, the time-lapse between the recordings was set as 0.5 s and those with multiple lasers were set at 1-3 s.

Note that primary hippocampal neuronal dendrites have a mixed polarity system, with the minus-end out for approximately one third of dynamic microtubules (Kapitein and Hoogenraad, 2011; Yau et al., 2016) and with the uniform plus-end out array in distal dendrites (Baas et al., 1988). To remove any effect of microtubule polarity during comparisons of different dynamic parameters between control and knockdown or overexpression systems (Figures 1, 2, 4, and 5), we analyzed similar numbers of granules from different parts of dendrites. All dynamic transport parameters were solely calculated from uni-directionally moving granules.

Imaging and movie analysis

Tracking of endogenous Rac1 RNA or TDP-43 protein

Experiments were carried out using one laser at a time. The time-lapse movies were analyzed using Imaris program 8.4.1 (Bitplane Science software, South Windsor, CT) with the manual particle-tracking module. Only granules with diameters $\leq$ 800 nm were analyzed. Notably, almost all granules with diameter > 800 nm were stationary. Granules that moved more than 3 μm in one direction within our tracking time-period of 10 s (0.5 s/frame) were considered as moving uni-directionally, whereas those exhibiting movement of at least 1 μm in either direction were considered bi-directional. Granules that moved less than 1 μm were considered stationary. Dynamic parameters, e.g., directionality of movements, net displacements and average velocities, were solely calculated from uni-directional granules.

Tracking of endogenous Rac1 mRNA along with endogenous or exogenous protein(s)

These experiments were carried out by simultaneous excitation with two or three lasers. Movie analysis and the criteria for assigning granule types were essentially as described above, except that in these cases the tracking time-period was ~15 to 30 s (1-3 s/frame).

Tracking of reporter RNA (TRICK-Rac1-3′UTR or MS2-Rac1-3′UTR) granules

Simultaneous excitation by two lasers was required to track co-movements of MCP-RFP and PCP-GFP associated with the un-translating reporter RNA granules. The criteria for assigning granule types were similar to those for the endogenous mRNA system, but the tracking time-period was ~30 s (2 s/frame). For translation kinetics of reporter RNAs, we analyzed the change in color (yellow to red) of TRICK reporter granules present in proximal (0-30 μm from soma) and distal (60-90 μm from soma) dendrites within 7-min time-periods. To analyze translation dynamics of Rac1 reporter RNA, we followed the individual un-translating (UT, yellow) granules until they became translating granules (TL, red). A granule was considered to pause if it appeared to be stationary or moving bi-directionally in the spine base region (3 μm) within the time-period of our real-time observation. It was considered translating (TL) when more than 50% of its fluorescence became red. All images were analyzed after subtraction of the background for each channel. Since the human retina is more sensitive toward green than red, many of the UT granules appeared to be green rather than yellow. When verified by visualizing raw images using two separate channels, most of these granules were found to be associated with red MCP-RFP protein.

Distribution of TL and UT TRICK-Rac1 3′UTR RNA granules in neuronal dendrites

For live-imaging, we identified the localization of pre-TL granules (those that were already red before detection) out of plane within neuronal dendrites as being the localization of synapses, which included the spine base (in plane) and the dendritic spine (out of

plane). We then followed the fate of individual TRICK granules within a radius of 5 μm of the synapse (representing an average of two dendritic spines). All images were analyzed after subtraction of the background for each channel.

Kymographs

Kymographs were generated for the transport dynamics of the endogenous Rac1 mRNP granules in Sc oligo-, TDPsi oligo-, FMRPsi oligo-, and Staufen1si oligo-transfected neuronal dendrites using MetaMorph software (Molecular Devices, USA). X-axes represent the length (70 μm) of the dendrite analyzed, whereas the y axis represents the time-period (300 s) analyzed.

QUANTIFICATION AND STATISTICAL ANALYSIS

Bar diagrams and pie charts were generated in Microsoft Excel. Statistical analyses were performed using GraphPad QuickCalcs (GraphPad Software Inc., La Jolla, CA). Student's t tests were carried out to compare the means, *$p < 0.05$, **$p < 0.001$, ***$p < 0.0001$. Categorical variables e.g., those represented by pie charts, were further compared using Fisher's exact tests. Specific details of biological and technical replicates are provided in the respective figure legends.

DATA AND CODE AVAILABILITY

No new datasets/codes were generated in this study.